

University of Alberta

Development of Surrogate Spinal Cords for the Evaluation of Electrode
Arrays Used in Intraspinal Implants

by

Cheng Cheng

A thesis submitted to the Faculty of Graduate Studies and Research

in partial fulfillment of the requirements for the degree of

Master of Science

in

Materials Engineering

Department of Chemical and Materials Engineering

©Cheng Cheng

Spring 2012

Edmonton, Alberta

Permission is hereby granted to the University of Alberta Libraries to reproduce single copies of this thesis and to lend or sell such copies for private, scholarly or scientific research purposes only. Where the thesis is converted to, or otherwise made available in digital form, the University of Alberta will advise potential users of the thesis of these terms.

Abstract

A surrogate spinal cord was developed to test the mechanical stability of electrode arrays for intraspinal implants. The mechanical and surface properties of candidate materials were tested. The elastic modulus was characterized using dynamic mechanical analysis. Forces required to indent the surrogate cords to specified depths was measured. Frictional forces were measured by pulling a needle out at a controlled rate. The results were compared to actual spinal cords, either to value from literature or *ex vivo* measurements. Surrogate cords with the most suitable properties (formaldehyde crosslinked gelatin, 12 wt% in water) were implanted with two types of intraspinal electrode arrays (one made of individual microwires and another of microwires anchored with a solid base), and an elongation was applied. Arrays with solid bases impeded the deformation of the cord suggesting that they could cause tissue damage *in vivo*, while arrays without a base moved freely with the cord.

Acknowledgement

I would like to express my heartfelt gratitude to Dr. Anastasia Elias, my supervisor, for her encouragement and guidance throughout my experiment and thesis writing processes. This thesis cannot reach to this form without her consistent and illuminating instructions.

I really appreciate Dr. Vivian Mushahwar, Dr. Walied Moussa and Dr. Kathryn Todd for their valuable suggestions and guidance for my research. I also want to thank the team members of the AHFMR SMART Team (etc. Imad Khaled and Jonn Kmech) for their help and collaborations.

Last my thanks would go to my family members for their considerations and confidence in me. I also want to acknowledge my boyfriend Jingxing Wei for his love and continuous support. I also owe my gratitude to my labmates, my friends and my fellow classmates who gave me their help to work out my problems during the difficult course of the thesis.

Table of Contents

Chapter 1 Introduction -----	1
1.1 Introduction to spinal cord -----	2
1.1.1 The spinal column segments -----	2
1.1.2 Rough anatomy and composition of the spinal cord-----	3
1.2 Spinal Cord Injury -----	5
1.2.1 Effects of Spinal Cord Injury -----	5
1.3 Previous methods developed to restore moving function after SCI -----	6
1.3.1 Surface electrical stimulation-----	6
1.3.2 Implanted muscle based FES system -----	7
1.3.3 Intrafascicular multielectrode stimulation (IFMS) -----	9
1.4 Intraspinal Microstimulations (ISMS) -----	10
1.4.1 Brief introductions to ISMS-----	10
1.4.2 Challenges of ISMS-----	12
1.4.3 Electrode arrays commonly used in neuron prostheses -----	14
1.4.3.1 The Utah Array-----	15
1.3.3.2. The McCreery array-----	17
1.4 Motivation -----	19
1.5 Road map -----	20

1.6 References	22
Chapter 2 Background	28
2.1 The mechanical properties of spinal cord	28
2.1.1 Mechanical property definitions	28
2.1.1.1 Elastic, viscous and viscoelastic materials	28
2.1.1.2 Elastic modulus, tensile modulus	31
2.1.1.3 Quasistatic mechanical properties and pseudo modulus	32
2.1.1 Characterization methods	34
2.1.2 Mechanical properties in the literature of animal and human spinal cords	37
2.1.2.1 Mechanical properties of spinal cords reported in the literature	37
2.1.2.2 The influence of measurement conditions on the results	40
2.1.3 Target modulus for the surrogate spinal cord	41
2.2 Previous research on the surrogate spinal cords	42
2.2.1 Surrogate cords made by silicone elastomers	43
2.2.2 Surrogate cords made by gelatin	47
2.2.3 Shortcomings of the previous surrogate spinal cords	50
2.3 References	53
Chapter 3 Materials selection	56
3.1 Candidate materials and sample preparation	59

3.2 Construction of surrogate spinal cord	60
3.3 Characterization of surrogate spinal cord materials	62
3.3.1 Dynamic Mechanical Analysis (DMA)	62
3.3.2 The indentation tests	69
3.3.4 Frictional Force Testing	77
3.5 Conclusions	85
3.4 References	88
Chapter 4: Deformation testing of the surrogate spinal cord	89
4.1 Deformation of human spinal cord	89
4.2 Electrodes for the deformation tests	91
4.2.1 Electrode arrays with individual wires	91
4.2.2 The McCreery array (solid base array)	92
4.3 Methods and results	94
4.4 Discussion and conclusions	105
4.4.1 Discussion	105
4.3.2 Conclusions	108
4.5 References	109

Chapter 5 Conclusion 110

5.1 References 113

List of Tables

Table 2-1: Spinal cord measurements from the literature -----	39
Table 2-2: Summary of the previous surrogate spinal cords -----	52
Table 3-1: Average tensile moduli and standard deviations of Sylgard 184 at mixing ratios (elastomer: crosslinker) of 10:1, 20:1, 30:1 and 40:1-----	64
Table 3-2: Average tensile moduli and standard deviations of 40:1 Sylgard 184, TCB 5101 and QM Skin 30 -----	65
Table 3-3: Tensile moduli of uncrosslinked and formaldehyde crosslinked 9 wt%, 12 wt% and 15 wt% gelatin in water -----	67
Table 3-4: Raw force vs. displacement data for the spinal indentation experiments for silicone cords and the rat spinal cords -----	72
Table 3-5: Raw force data for the spinal indentation experiments for formaldehyde crosslinked hydrated gelatin cords and the rat spinal cords -----	75
Table 3-6: Summary of the statistical analysis. -----	76
Table 3-7: Average peak frictional stresses of the candidate materials -----	81
Table 4-1: Observed strain in reference samples (without electrodes) under 12% tension -----	98
Table 4-2: Observed strain in reference samples with individual microwires under 12% tension -----	100
Table 4-3: Observed strain in reference samples with solid base array under 12% tension -----	102

Table 4-4: Comparisons of the calculated strains to the observed strains of the surrogate spinal cord with the individual microwires, solid base array and without any arrays (reference cord)-----105

List of Figures

Figure 1-1: Schematic of the human spinal cord-----	3
Figure 1-2: Transverse section drawing of human spinal cord at C8 -----	4
Figure 1-3: Schematic of the meninges of human spinal cord -----	4
Figure 1-4: Schematic of the CWRU/VA implanted neuronprostheses system -----	9
Figure 1-5: Schematic representative location of ISMS implantation -----	11
Figure 1-6: Schematic of the microelectrodes with their tips implanted into the ventral horn of spinal cord -----	13
Figure 1-7: A scanning electron micrograph image of the Utah electrode array -----	16
Figure 1-8: A scanning electron micrograph image of the platinum coated tips of the UEA electrodes -----	16
Figure 1-9: A scanning electron micrograph image of the slanted Utah array -----	17
Figure 1-10: (A) A representative McCreery array for deep brain stimulations. (B) A representative McCreery array for spinal cord implantation, which as used for feline sacral spinal cord -----	18
Figure 2-1: Stress-strain behaviors of (a) pure viscous material and (b) viscoelastic material under sinusoidal applied strain -----	30
Figure 2-2: Schematics of tensile modulus -----	32
Figure 2-3: Stress-strain curves for (a) human cervical spinal cord and (b) rat spinal cord at different strain rates -----	34

Figure 2-4: A typical tensile testing setup for spinal cord -----	35
Figure 2-5: Representative human spinal cord specimen -----	38
Figure 2-6: Comparisons of <i>ex vivo</i> human spinal cord with and without <i>pia mater</i> -----	41
Figure 2-7: The general structure of silicone elastomers -----	44
Figure 2-8: Example of the applications of silicone elastomers as skin substitute in biomaterials engineering -----	45
Figure 2-9: Surrogate spinal cord made by QM Skin 30 -----	46
Figure 2-10: Molecular structure of (a) proline, (b) glycine and (c) one typical repeat unit of gelatin -----	47
Figure 2-11: Scanning electron micrographs of (a) gelatin microspheres for drug delivery (b) Cross-sectional of a 3D chitosan–gelatin–chondroitin scaffold -----	49
Figure 2-12: The comparison of the stress-strain behavior of different wt% gelatin samples and the feline spinal cords (the shaded area) under compression. Adapted from -----	50
Figure 3-1: Schematic for the aluminum mold for producing the surrogate spinal cords with its dimensions -----	60
Figure 3-2: MRI image of feline spinal cord. (Provided by Vivian Mushahwar in Cell Biology Department) -----	61
Figure 3-3: Representative image of a surrogate spinal cord in a petri dish -----	61
Figure 3-4: Picture of DMA 8000 -----	62
Figure 3-5: Tensile moduli of Sylgard 184 at mixing ratios (elastomer: crosslinker) of 10:1, 20:1, 30:1 and 40:1-----	64

Figure 3-6: Tensile moduli of 40:1 Sylgard 184, TCB 5101 and QM Skin 30 ----	65
Figure 3-7: Tensile moduli of uncrosslinked and formaldehyde crosslinked gelatins with 9 wt%, 12 wt% and 15 wt% gelatin in water -----	67
Figure 3-8: Photos of the setup for indentation test -----	71
Figure 3-9: The average force of indentation required achieving specific displacements of different silicone cords and the rat spinal cords-----	73
Figure 3-10: The average force of indentation required achieving specific displacements of formaldehyde crosslinked gelatin at different weight percent in water -----	76
Figure 3-11: Schematic of the frictional force testing set-up during needle insertion -----	78
Figure 3-12: A typical force vs. displacement curve for one test recorded from a QM Skin 30 surrogate cord -----	80
Figure 3-13: Average peak frictional stresses of the candidate surrogate spinal cord materials -----	82
Figure 3-14: Comparisons of the peak frictional stress of formaldehyde crosslinked 12 wt% gelatin in water and 40:1 Sylgard 184 obtained from the shorter distance and longer distance measurements -----	83
Figure 4-1: Strains of anterior and posterior surfaces of the entire cervical spinal cord at different head flexion angle of the five volunteers -----	91
Figure 4-2: Picture of the individual microwires implanted in the formaldehyde crosslinked 12 wt% gelatin in water surrogate cord -----	92

Figure 4-3: Picture of the McCreery arrays implanted in the formaldehyde crosslinked 12 wt% gelatin surrogate spinal cord -----	93
Figure 4-4: Picture of the Teflon stand for the deformation testing -----	94
Figure 4-5: Surrogate spinal cords (a) implanted with individual microwires; (b) implanted with electrodes held with solid base; and (c) reference cord with no implants -----	97
Figure 4-6: Strain of L1, L2, L3 and L4 of surrogate cord without electrodes implanted under 12% tension -----	99
Figure 4-7: Strain of L1, L2, L3 and L4 of surrogate spinal cord with individual microwires implanted under 12% tension -----	100
Figure 4-8: Strains observed in surrogate spinal cords implanted with McCreery arrays, subjected to 12 % tension -----	103
Figure 4-9: Comparisons of the strains of the cord with individual microwires, solid base array and without any array between L1 to L5-----	104
Figure 4-10: Picture of the flexible array developed by Imad Khaled -----	
107	

Chapter 1 Introduction

Spinal cord injuries can permanently damage the signal connection pathway in the central neuron system, resulting in a partial or complete loss of motion and feeling in the body lower than the point of injury. Many clinical attempts have been made to restore partial function after spinal cord injuries. A promising technique uses electrical stimulation to pass signals to the neurons lower than the point of injury so as to activate the muscles. My collaborators are investigating the use of intraspinal microstimulations (ISMS) to restore standing and walking functions in patients with spinal cord injuries (SCI). In this technique, fine microwires are inserted into the spinal cord to stimulate the signals of the healthy neurons below the point of injury. Ideally, microelectrode arrays are needed for stimulating multiple neurons within a defined pool. Currently one of the crucial challenges of ISMS is to design appropriate microelectrode arrays which have suitable electronic properties and biocompatibility. Typically, metal or silicon electrodes are used in these types of arrays; however the stiffness of these materials is much higher than that of the spinal cord, which is very soft and delicate. Therefore, the mechanical compatibility of the microelectrode arrays employed in ISMS must be carefully considered. The goal of my study is to develop an *in vitro* proof-of-concept spinal cord model to test the mechanical suitability of both existing electrode arrays (which have been developed for use in the brain) and new arrays being developed in my research team. This model could also potentially be used to test other types of implants being developed for the central nervous system.

In this chapter, basic knowledge of spinal cord and spinal cord injuries (SCI) will be described. Methods currently used to treat SCI will also be introduced. Finally, an overview of the technique of ISMS and of the currently available electrodes will be given to provide context for the research described in this thesis.

1.1 Introduction to spinal cord

The spinal cord is a long, tubular organ with an elliptical cross section that contains both nervous tissue and other support cells. It is part of the central nervous system which connects the brain to the lower body by carrying both signals from the brain to the muscles in the lower body, and sensory information from the lower body to the brain. The neurons in the spinal cord relay signals both chemically and electrically.

1.1.1 The spinal column segments

In humans, the average total length of spinal cord is about 45 cm for an adult male and about 43 cm for an adult female [1]. A schematic of the human spinal cord is shown in Figure 1-1. The spinal cord is very soft and is protected by the spinal column which has a curved shape [2-4]. There are 31 segments of human spinal cord, 7 cervical segments (C1- C7 but 8 cervical nerves), 12 thoracic segments (T1-T12), 5 lumbar segments (L1-L5), 5 sacral segments and 1 coccygeal segment. The width of the spinal cord varies at different segments, with the widest measuring about 12 mm in the cervical [1] and lumbar regions and the narrowest of about 6 mm at thoracic region [5]. The spinal column is used to protect the delicate spinal cord, and the cord and the column move independently of each other.

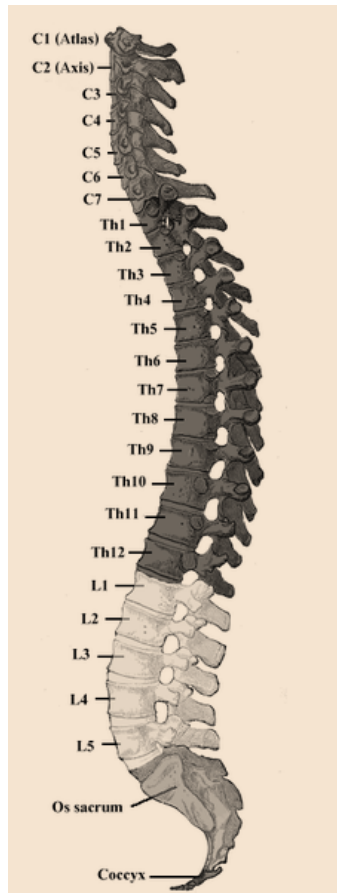


Figure 1-1: Schematic of the human spinal cord. There are 8 cervical vertebrae (C1-C8), 12 thoracic vertebrae (T1-T12), 5 lumbar vertebrae (L1-L5), 5 sacral vertebrae (S1-S5), and 1 coccygeal vertebrae [6].

1.1.2 Rough anatomy and composition of the spinal cord

There are two main tissue networks inside the spinal cord: *gray matter* and *white matter* (shown in Figure 1-2). The *gray matter* is located in the butterfly-like area of the spinal cord which contains the dorsal horn and the ventral horn. It is a very complex structure with organized layers of cells, including neuron cell bodies, dendrites, axons and glial cells [7-9]. The *white matter* is located outside the butterfly-like area of the spinal cord. Most of the *white matter* is composed of

longitudinally running axon fibers and glial cells which carry signals from or to the brain.

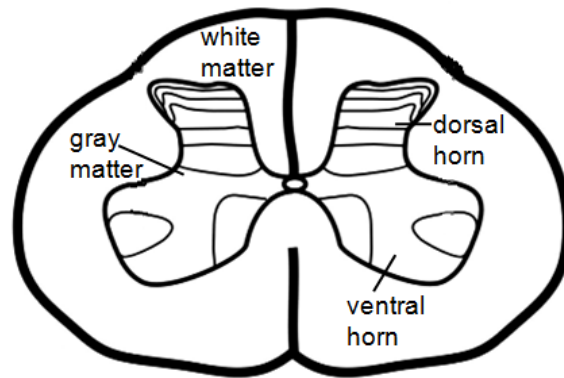


Figure 1-2: Transverse section drawing of human spinal cord at C8. The main components of the spinal cord (*gray* and *white matter*) are labeled. The central canal lies in the center of the *gray matter*. The *white matter* is located outside the gray matter.

Adapted from [10]. Reprinted with the copyright permission from Elsevier Ltd.

There are three layers surrounding the spinal cord tissue, namely the meninges of spinal cord. The outermost layer is called *dura mater*. It is stiff and inflexible to keep in the cerebrospinal fluid (CSF). The innermost layer, the *pia mater*, is a hard, fibrous layer which is impermeable to fluid [11], with a thickness of less than three hundred microns [12]. There is a spider-web like layer in between of the *dura* and *pia mater*: the *arachnoid mater*. The meninges of spinal cord both protect the spinal cord and keep the CSF surrounded to keep the right environment [13]. A schematic of the spinal cord meninges is shown in Figure 1-3.

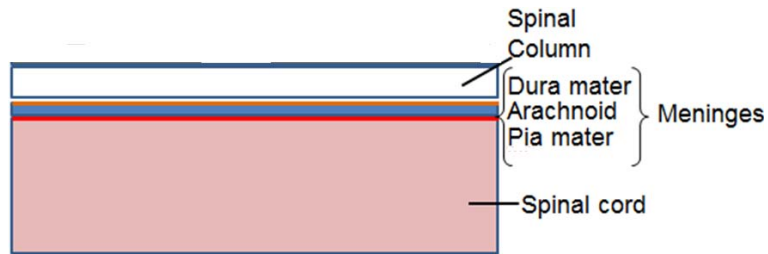


Figure 1-3: Schematic of the meninges of human spinal cord.

1.2 Spinal Cord Injury

1.2.1 Effects of Spinal Cord Injury

Spinal cord injury (SCI) is part or complete damage of the spinal cord caused by trauma, and cannot be reversed. SCI causes partial or complete loss of motion and sensations in the body lower than the point of injury, which in turn disrupt the patient's life quality and health, and can even cause secondary disabilities such as heart disease [14, 15], diabetes [14], muscle atrophy [16, 17] and bone fracture [18, 19]. Anderson also showed that the quality of life of patients with SCI was largely affected by the psychological and sociological influence of both SCI and its secondary diseases [20].

Nowadays, about 86,000 Canadians are living with spinal cord injury. This causes an estimated economic burden of \$3.6 billion each year including \$1.8 billion for direct health care costs according to the Rick Hansen Institute and the Urban Futures Institute in Quebec [21]. In the United States, the United Spinal Association reported that the number of people with SCI was estimated to be between 222,000 and 285,000, with about 11,000 new cases each year. In 1996,

the total annual cost of SCI in the United States was estimated to be \$9.73 billion, including approximately \$2.6 billion in lost productivity [22].

The main causes of SCI can be attributed to traffic accidents, sports, falls and other reasons according to research from the United States [22]. It has also been shown that the total number of male patients suffering from SCI is much greater than the number of female patients [21, 22].

1.3 Previous methods developed to restore moving function after SCI

The reason why SCI permanently damages the connectivity of the brain and the lower body is that the neuron cells, which carry the electrical and chemical signals, are not repairable after death. Research into functional electrical stimulation (FES) began decades ago, and the goal of this research is to stimulate the muscles electrically to restore partial motor function by stimulating nerves which control the desired muscles [23-36]. This treatment is still under development today. FES applies electrical signals to stimulate neuron cells lower than the point of injury. Four different types of FES have been developed to try to treat with spinal cord injury [23], each of which will be introduced below, in the order from least invasive to most invasive.

1.3.1 Surface electrical stimulation

Surface electrical stimulation was the first method in FES for use in the treatment of spinal cord injuries. It requires using one set of surface electrodes directly

attached to the skin over nerves to activate muscles for the motion of knee and hip, and another set of surface electrodes to trigger a flexor withdrawal reflex. The proof-of-concept of surface electrical stimulation was reported in 1961 as treatment to hemiplegia (the inability to move a group of muscles in one side of the body) [24] rather than as a treatment of spinal cord injury, and in this study, it was shown that the surface electrodes could activate limited movements of the muscle. The first attempt to treat thoracic spinal cord injury was by Kralj *et al.* [25] and the results showed that moderate movements could be generated. Surface electrical stimulations have been put into clinical experiments, and also commercialized [26]. However, to date, surface electrode stimulation can only restore a moderate range of standing and walking functions for patients. Since the electrodes are attached to the surface of the skin and the stimulator must be carried during the treatment, the patient must move very carefully in a relatively neat and clean environment to prevent the surface electrodes from being damaged or dislodged. Another drawback of surface electrical stimulation is that it is difficult to target the desired muscles since the electrodes are on the surface while some of the desired muscle may be deep inside the skin. Finally, if nerves are repeatedly stimulated for a long-term for activation of the muscle, the stimulation may affect its ability to generate stable movements, resulting in fatigue.

1.3.2 Implanted muscle based FES system

To improve the complicated environmental requirements of surface electrical stimulations, researchers in Case Western Reserve University (CWRU) and the

Department of Veterans Affairs (VA) developed an *implanted* muscle based stimulation system as a treatment for low cervical and thoracic injuries [27]. A brief schematic of this system is shown in Figure 1-5. The system contains an implantable intramuscular electrode targeted at the epimysial sheath (the external sheath of connective tissue surrounding a muscle), in-line connectors and a pulse generator (which need to be implanted as well) [27-29]. Apart from helping the patients with incomplete SCI with standing by stimulating at the hip, knee and the foot-ankle muscles, the system can also restore partial movement by stimulating the muscles which control the desired motion. Although surgery is required for this system, it is much more convenient than the surface electrical stimulation systems, since after the implantation it is securely fixed to the muscles. This system has already been used in clinical trials, and it has been found that the system is stable and safe for most patients for at least about 6 years [30]. Users have also reported positive satisfaction with the system. However, there are also disadvantages to this technique. First, since the electrodes are inserted directly into the motor neuron around targeted muscles, the stimulation will cause the targeted muscle to fatigue over time. Furthermore, only parts of the desired muscles are activated by this approach, since the neuron cells around the muscle controls only certain locomotor functions.

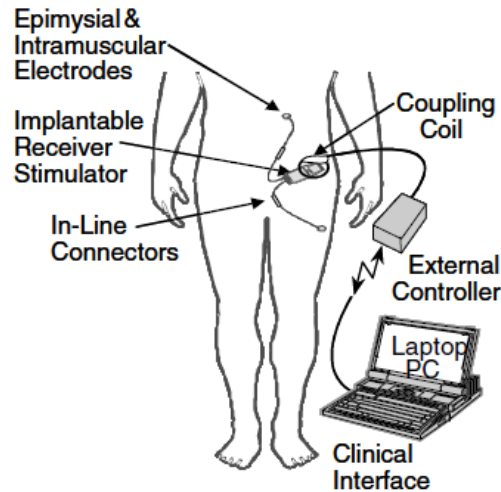


Figure 1-4: Schematic of the CWRU/VA implanted neuronprosthesis system [23].

Reprinted with the copy right permission of Institute of Physics (IOP).

1.3.3 Intrafascicular multielectrode stimulation (IFMS)

IFMS was developed by researchers at the University of Utah [32-34]. It requires the insertion of multi-site microelectrode into multi nerve fascicles (bundles of skeletal muscle fibers surrounded by connective tissue). Therefore, the target muscles can be activated through the stimulation of the related fascicles instead of stimulation of the entire muscle tissue. The main advantage of IFMS is that it is fatigue-resistant, since the motor-units are activated independently and are not activated when they are not actually needed in a specific motion. IFMS implantation has been demonstrated in cats, and it has been shown that this technique can generate muscle force which was physiologically proved to be fatigue-resistant [32-34]. While these experiments have only been carried out on animals such as cats, IFMS could potentially be a treatment for individuals with SCI. However, the complication of the stimulator caused by inserting large

numbers of electrodes into the peripheral nerves make the control and modification of the stimulator parameters such as times and steps extremely difficult. Although the force generated has shown to be fatigue-resistant, the long-term influence of multi-site microelectrodes on requires further investigation.

1.4 Intraspinal Microstimulations (ISMS)

My collaborators utilize intraspinal microstimulation (ISMS, the fourth type of functional electrical stimulation) to restore functions after SCI. In this section, the basic principles and main advantages of ISMS will be introduced, and the main challenges for the utilizations of ISMS will be addressed.

1.4.1 Brief introductions to ISMS

Intraspinal microstimulation is another promising technique for attempting to restore standing and walking function after SCI. This technique requires inserting fine microelectrodes into the tissue of spinal cord [37, 38]. Electrical signals can then be directly passed on to the healthy spinal cord tissue lower than the point of injury, and the neurons in the tissue can transmit these signals to the relevant muscles. The main difference between ISMS and other stimulation methods to restore function after SCI is that ISMS focuses on simulating the central nervous system instead of the muscle in the lower body. ISMS reduces the potential of the implanted electrodes to damage the muscle since the electrodes are not inserted directly into the muscle. The electrode arrays can be protected by the spinal column surrounding the spinal cord. In this way, the probability of dislodging the

electrodes during stimulation can be reduced (as compared with inserting the electrodes into the muscles).

The target region for ISMS implantation is the lumbosacral enlargement. The reason why this region was chosen is that the ventral horn within it contains pools of motor neurons which activate all the muscles in the lower body [35] as well as a large portions of the neuronal networks that control locomotion [36]. The representative implantation location is shown in Figure 1-6.

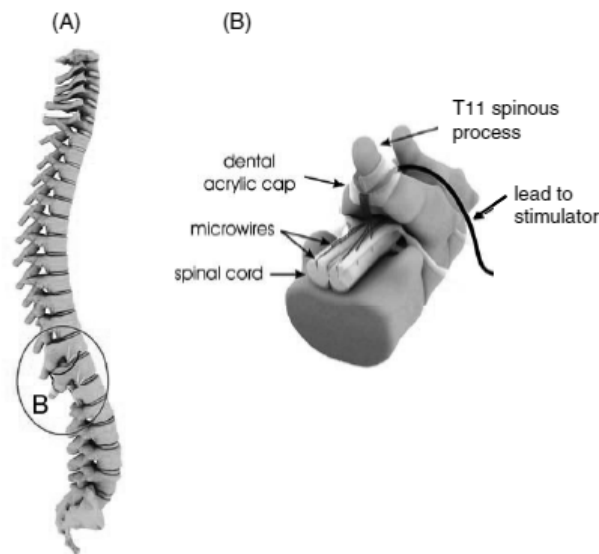


Figure 1-5: Schematic representative location of ISMS implantation (A) A schematic of human spinal column with lumbosacral region circled which is the target region of ISMS implantation. (B) A schematic of the ISMS implant in detail [23]. Reprinted with the copyright permission from Institute of Physics (IOP).

So far, clinical experiments of ISMS have not been undertaken on human patients with SCI. Preliminary experiments have been conducted on animals, particularly cats [37-43] and rats [44], since in these animals the distribution of motor neurons

within the ventral horn is very similar to humans [39, 45-47]. These experiments have shown that ISMS is capable of generating stepping similar to locomotion and movements controlled by feedback [40] and activating similar movements to those by stimulating nerve or muscle directly [42].

There has also been research focused on the stability, efficiency and reliability of ISMS system of animals. The ISMS system has been proved to function with good electrical stability in cats for at least 6 months [48], and after 6 months implantation no significant chronic inflammation of the surrounding tissue was observed [49]. Another study by Lau *et al.* [50, 51] showed that long-term, weight-bearing standing can be produced using ISMS with less than 3% of the current needed for intramuscular stimulation. To examine biological response to electrodes, Bamford *et al.* [10] used 30 micron diameter platinum iridium individually inserted electrodes to test the tissue response of rats during 30 days' stimulations and found that there is only minimal damage to the cord biologically. All of the studies have showed that ISMS may have the potential to restore the movements of limbs for the long-term after spinal cord injury.

1.4.2 Challenges of ISMS

There are still some critical challenges for ISMS. First, the microwires need to be accurately targeted to the motor neuron pools in the ventral horn of the lumbosacral spinal cord (shown in Figure 1-7 (a)). The targeting of the electrodes requires using MRI (Magnetic Resonance Imaging) to image the specific spinal cord, and then to use these images to determine the insertion location, depth and angle

required to reach the desired neurons. If the electrodes are not inserted accurately or are inserted at an angle, they may miss their target tissue. With respect to the miss-targeting of electrodes, it is estimated that the accuracy of ISMS wires insertion is within about 1 mm of the targeted tissue [52]. Inaccurately inserted wires will prevent the appropriate muscular responses or other undesirable responses like flexor withdrawal response for pain [23]. Furthermore, it is desirable that the electrodes remain implanted over the long-term. It is therefore of extreme importance that the electrodes must not become dislodged from the correct position over time. This makes the design of proper electrode crucial to the success of ISMS.

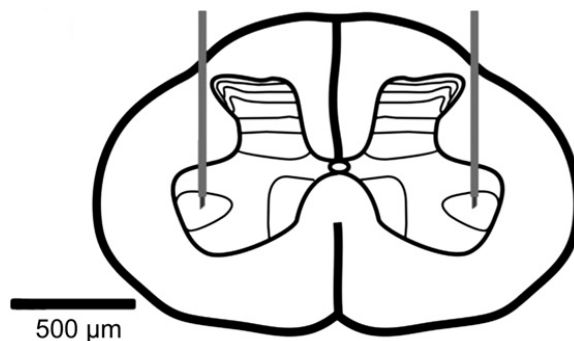


Figure 1-6: Schematic of the microelectrodes with their tips implanted into the theventral horn of spinal cord [10]. Reprinted with the copyright permission from Elsevier Ltd.

Another challenge is the mechanical influence of the implanted microelectrodes on the spinal cord tissue. Although the implantation of individual 30 μm Pt-Ir electrodes in the rat spinal cords for 30 days has showed no significant damage to the spinal cord [10], long-term stability and compatibility must be proven.

Currently, the size of the electrodes chosen for implantation is limited to between

30-80 μm in diameter, as research has shown that tissue damage can be minimized during the insertion process if the electrodes have diameters of less than 50 μm , and if they are highly flexible [49]. During daily motion, the spinal cord undergoes flexing, stretching, bending and twisting etc. For example, it is estimated that the average maximum strain of human cervical spinal cord is 12% [53]. If there are relative movements between the spinal cord and electrodes, stress would occur on the interface, which may cause damage to the spinal cord tissue mechanically during long-term implantation.

Another practical concern is that currently, for ISMS, the surgeon must insert 6-12 electrodes individually [23], which is tedious and may cause inconsistency. This process can be improved by using microelectrode arrays (in which the electrode are connected together), many of which are described in the literature [54]. Various electrode arrays that could potentially be used in ISMS will be discussed in the next section.

1.4.3 Electrode arrays commonly used in neuron prostheses

The design of microelectrode arrays is crucial for the development of ISMS. Numerous electrode arrays have been developed for implantation into the brain to both stimulate and record signals from neurons. Some of these arrays *may* be useful in the spinal cord. The most commonly used electrode arrays are the Utah array and the McCreery array. In this section, a brief introduction will be made to each of these arrays, and their applicability to spinal cord implantation will be discussed.

1.4.3.1 The Utah Array

Before the invention of the Utah array, deep brain stimulation was achieved by surgically inserting individual microwires into the motor cortex region of the brain [55]. Researchers at University of Utah designed and developed a process to build a 10 x 10 electrode array which could be implanted all at once [56]. An SEM picture of the Utah array is shown in Figure 1-8 [57], and a close-up image of the tips of the electrodes is shown in Figure 1-9 [57]. A typical Utah Electrode Array consists of 100 silicon penetrating electrodes, arranged in a 10 x 10 grid (16 mm²) on a 0.2 mm thick silicon substrate. The length of each electrode is 1.5 mm. The electrical access to each electrode is provided by a gold contact pads on the back of the array. Since silicone is insulated, the surfaces of the electrodes are metalized with platinum to facilitate the passing of current to the gold pad.

The Utah array has been used in many cases in deep brain implantation. It has been implanted in the cerebral cortex [56] to stimulate interconnected neurons within a small range of the brain [58]. This array has been shown to best able enough to be used in chronic recording, and 60% of the electrodes in one array can still function after 6 months [59]. The slanted Utah array, whose depth of electrodes increases gradually in different rows (shown in Figure 1-10) has even been used in spinal cord implantation [32]. However, the long-term performance in a chronic application within the spinal cord has not been studied. In addition, the silicon base is very stiff, so its influence on the spinal cord tissue is unknown but is a cause for concern.

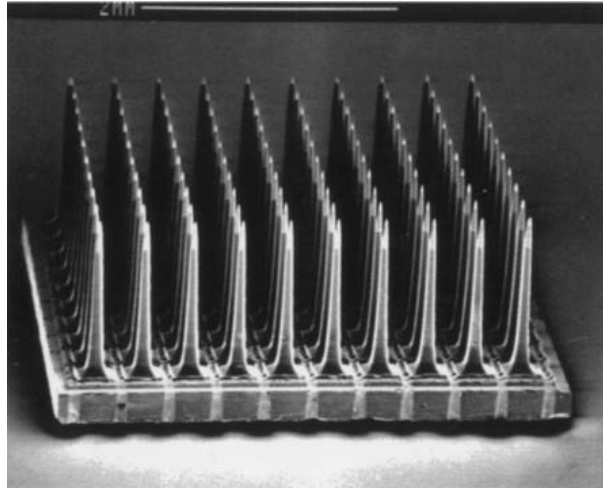


Figure 1-7: A scanning electron micrograph image of the Utah electrode array (10 x 10)(UEA) [57]. Reprinted with the copyright permission from Elsevier Ltd.

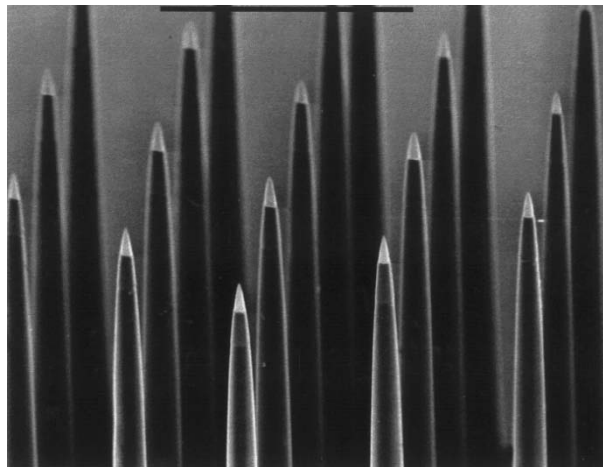


Figure 1-8: A scanning electron micrograph image of the platinum coated tips of the UEA electrodes. Scale bar measures 0.5 mm [57]. Reprinted with the copyright from Elsevier Ltd.

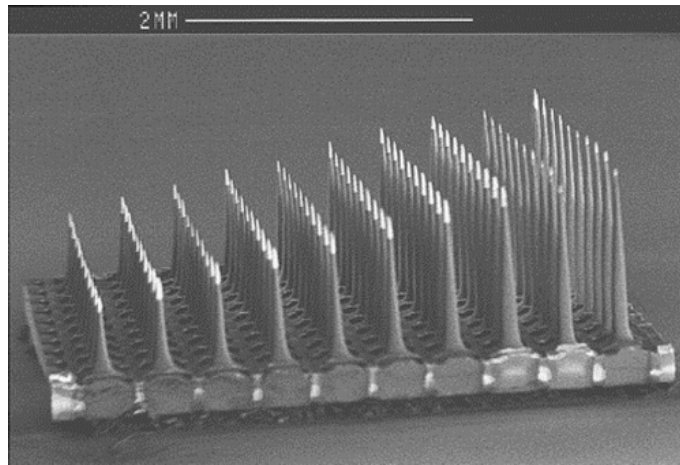


Figure 1-9: A scanning electron micrograph image of the slanted Utah array [60].

Reprinted with the copyright permission from Annual reviews, Inc.

1.3.3.2. The McCreery array

Another type of electrode arrays is the McCreery array, which was developed at the Huntington Medical Research Institute in 1983. This array was first used for the recording and stimulation of neurons in the feline brain, and it was proved that this array has a very high efficient of recording signals and stimulating central neuron cells [61]. Another application in which the McCreery array has been used is in the restoration of hearing function, by the stimulation of ventral cochlear cells [62]. Recently this array has been implanted into feline spinal cord for a short term (less than 6 months) to restore the control of bladder and bowel [63, 64]. The McCreery array has been commercialized as a type of neural prosthesis. A typical McCreery array contains 2 or 3 rows of electrodes made of iridium and a stiff, solid epoxy base to hold the electrodes in place. It can be customized for different

dimensions and types of neuron tissue. The utilization of the solid base simplifies the surgical process, avoiding tedious insertion of each electrode. However, the utility of the McCreery array for use in ISMS is still uncertain due to several reasons. First, penetrating iridium electrodes held by solid base have the potential to cause tissue injury, both during the implantation process and during the subsequent long-term stimulations [65-67]. To date, no studies have been carried to evaluate the long-term mechanical influence of the electrode to tissue. Another concern is that the substrate material, epoxy, is very stiff and solid, which cannot respond when the spinal cord is deformed under the normal range. Therefore it may move relatively to the spinal cord itself, which may cause damage to the tissue since shear stress would occur at the interface between the electrode tips and the cord which may cause the cord to be torn in the long-term implantation, especially when the spinal cord undergoes lots of deformations during daily lives.

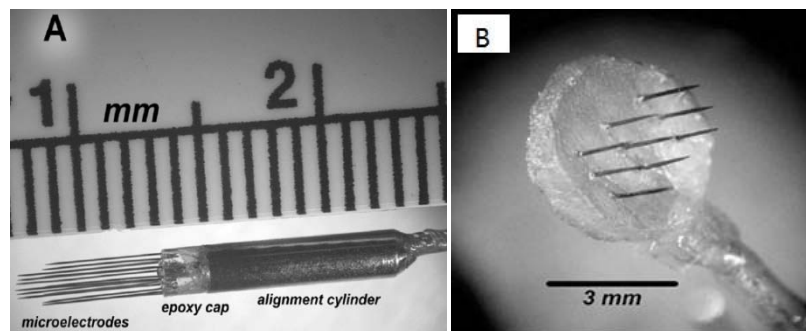


Figure 1-10: (A) A representative McCreery array for deep brain stimulations [68]. (B) A representative McCreery array for spinal cord implantation, which as used for feline sacral spinal cord [63]. Reprinted with the copyright permission grant of IEEE (from Microelectrode array for chronic deep-brain micro stimulation and recording by

McCreery D. et al. in IEEE Transactions on Biomedical Engineering [68] and Arrays for chronic functional microstimulation of the lumbosacral spinal cord by McCreery D et al. in IEEE IEEE Trans Neural Syst Rehabil Eng. [63]).

1.4 Motivation

The availability of appropriate microelectrode arrays is crucial for the development of ISMS, and currently the mechanical influence and stabilities of various available electrodes still requires evaluation. Aside from having stable stimulation properties, the selected arrays must have mechanical compatibility with the spinal cord tissue.

I am part of a group developing the utilization of ISMS for the treatment of spinal cord injury. In a previous experiment conducted by my collaborators, the McCreery was implanted into cat spinal cord to stimulate neurons. However, the treated cat was found to have paralysis within 1 month of implantation, possibly due to the mechanical mismatch between the cord and the array. Therefore, it is extremely important to test their biocompatibilities both biologically and mechanically.

Testing of the mechanical stabilities and interactions between the electrode arrays and actual excised spinal cords is impractical, both due to the difficulties and cost in the harvesting of spinal cords, and due to the fact that spinal cord tissue is fragile and difficult to handle, and degrades quickly after removal. Similarly, it is both undesirable and costly to test immediately in animals. Therefore, it is desirable to engineer a physical spinal cord model to facilitate the testing of designed arrays in the preliminary stage. The design can be modified based on the testing results.

When the design is mature enough, the testing could be switch to real animal spinal cords, and eventually human spinal cords.

There are two phases in the research described in this thesis. In the first phase, candidate materials for use in surrogate spinal cords were selected and evaluated, to identify a material which could mimic the properties of the real spinal cord. In the second phase of the work, surrogate spinal cords were used to test the mechanical stability of both existing and newly developed electrode arrays under deformations characteristic of daily motion.

1.5 Road map

This master's thesis contains five chapters. In Chapter 2, background information for engineering surrogate spinal cords is addressed. This chapter describes the previous research on the mechanical properties of the human and animal spinal cords. The target modulus for the surrogate spinal cord was chosen based on the literature review and discussions. Previous research on surrogate cords is also introduced to give a brief idea about the development of surrogate spinal cords. Chapter 3 describes the first phase of this research: the selection of a proper material from which to make surrogate spinal cords using various characterization techniques. Three types of silicone elastomers and different formulations of gelatin were characterized by three different methods and compared with the real spinal cords. A suitable candidate material was chosen based on all of these tests, and this material was subsequently used to make surrogate spinal cords for *in vitro* testing.

Chapter 4 describes the second phase of the research: the deformation of the surrogate cords with different types of arrays implanted. Two existing arrays were tested -one comprised simply of individual wires (without a base) and one type of McCreery array. The deformation of the cord was measured by imaging the cord optically before and during deformation.

The final chapter (Chapter 5) summarizes the conclusions of my work, and presents a brief outlook for future research.

Chapter 2 Background

2.1 The mechanical properties of spinal cord

Knowledge of the mechanical properties of real spinal cord is very crucial for the construction of a physical model to simulate the mechanical behavior of spinal cord.

The elastic and bulk compressive moduli, rheological properties and deformation behavior have been investigated by a number of researchers. This chapter describes the main methods and results of this research, explains why differences in moduli are seen in measurements made by different groups, and finally defines the target modulus for the surrogate spinal cord which will be developed as a part of this thesis work.

2.1.1 Mechanical property definitions

This section describes some definitions and terms [1] which will be used in the discussions on the mechanical properties of spinal cord.

2.1.1.1 Elastic, viscous and viscoelastic materials

When subjected to an applied force (or stress), a material can exhibit an elastic response, a viscous response, or a combination of both. To offset the influence of the applied force, an internal force is generated by the material called a restoring force. Stress is defined as the ratio of restoring force divided by the area over which the force is applied ($\sigma = F/A$). For purely elastic materials, there will be no residual strain ($\epsilon = l/l_o$) upon the removal of stress. Therefore the stress and the strain are exactly in phase.

However, for viscous materials, the shear flow and resistance will increase with time once a stress is applied. The corresponding strain will be out of phase, and there will be a 90 degree lag. Most polymers exhibit both elastic and viscous properties, and can be called viscoelastic materials. In this study, both real spinal cords and the candidate materials tested for the construction of surrogate spinal cords are viscoelastic materials. Therefore, there is some phase lag between the strain and the stress. The phase can be calculated from the following equations:

$$\text{Stress: } \sigma = \sigma_0 \sin(t\omega + \delta) \quad (2.1)$$

$$\text{Strain: } \varepsilon = \varepsilon_0 \sin(t\omega) \quad (2.2)$$

Where ω is frequency of strain oscillation, t is time, and δ is phase lag between stress and strain.

The stress responses to applied strain for both purely viscous and viscoelastic materials are shown in Figure 2-1.

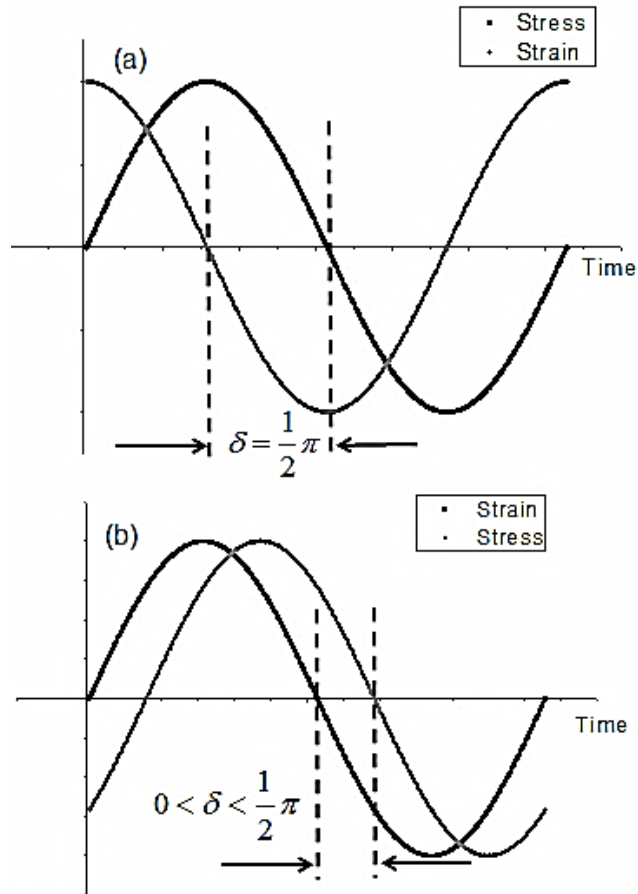


Figure 2-1: Stress-strain behaviors of (a) pure viscous material and (b) viscoelastic material under sinusoidal applied strain. The phase lags δ for each material is also shown. There is no phase lag for a purely elastic material. Adapted from [2].

Taking viscoelastic properties into account, a complex modulus is used to describe polymers. The complex modulus can be divided into two components. The storage modulus is the elastic portion, and measures the energy stored in the material. The loss modulus is the viscous portion, and measures the energy dissipated as heat.

$$\text{Storage modulus: } E' = \frac{\sigma_0}{\varepsilon_0} \cos \delta \quad (2.3)$$

$$\text{Loss modulus: } E'' = \frac{\sigma_0}{\varepsilon_0} \sin \delta \quad (2.4)$$

Phase angle, $\tan(\delta)$: $\tan \delta = \frac{E''}{E'}$ (2.5)

The complex modulus can be expressed as follows:

$$E = E' + iE''$$

Where $i^2 = -1$.

2.1.1.2 Elastic modulus, tensile modulus

The elastic modulus describes the material's tendency to be deformed in a recoverable way when subjected to a force. It is defined as the slope of the material's stress-strain curve in the region where they are exactly in phase. The definition is shown in

Equation 2.6 [3].

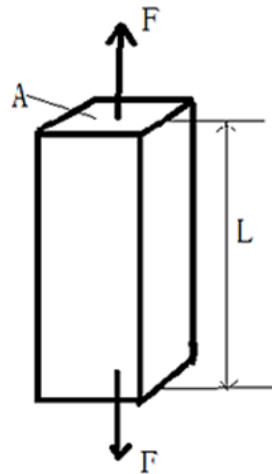
$$E = \frac{d\sigma_e}{d\varepsilon_e} \quad (2.6)$$

Where ε_e is the amount of strain recovering immediately after the removal of stress and σ_e is the amount of stress with the same phase as ε_e .

The strain rate is the slope of strain-time curve. For viscoelastic materials, the elastic modulus is influenced by the rate at which the strain is applied. Therefore, the rate at which the spinal cord is deformed can affect the modulus which is measured, as will be discussed in a later section.

There are different types of elastic moduli which can be measured under different conditions. Only the tensile modulus (E) is relevant to the characterization of the spinal cord. This modulus characterizes a material's tendency to deform along an axis upon when a tensile force is applied along that axis. The elastic part of the tensile

modulus (the linear portion of the stress-strain curve, which occurs when strain rate is low) is called Young's modulus, and is often referred to simply as the elastic modulus. It is defined as the ratio of tensile stress to tensile strain. The spinal cord is typically characterized in terms of the tensile modulus.



$$E = \frac{\sigma}{\varepsilon} = \frac{F / A}{(L_2 - L) / L} = \frac{FL}{A(L_2 - L)}$$

Figure 2-2: Schematics of tensile modulus. In the figure, F is the applied force; A is the area of the cross section, and L and L₂ are the length of material before and after deformation, respectively. Adapted from [1].

2.1.1.3 Quasistatic mechanical properties and pseudo modulus

Since spinal cord tissue is viscoelastic, the viscous part of material also contributes to the modulus. For the viscous part of the modulus, different strain rates will cause different impedances in the material. Thus the viscous part of the modulus varies with the strain rate. For example, Figure 2-3 (a) and (b) shows the stress-strain curves obtained at different applied strain rates for human spinal cords [4] and rat spinal cords

[5]. In this figure, the slope of the stress-strain curve for each measurement is representative of its modulus at that strain and strain rate applied according to Equation 2.6. It is shown that at different strain rates, different stresses were required to achieve the same amount of strain.

When characterizing spinal cords, the loading conditions have a large influence on the results. Several different types of measurements have been taken to measure the elastic or viscous properties of spinal cord [4-8]. When the applied strain rate is nearly 0, the loading conditions approach the quasistatic region, where the modulus is purely elastic. The mechanical properties measured under this condition are called quasistatic mechanical properties. To measure the viscoelastic properties of spinal cord, it is desirable to apply different (and relatively large) strain rates and compare the measured moduli [4, 5].

During the measurements of spinal cord [4, 5], a non-linear response is often seen, in so far as the modulus tends to increase as the strain rate increases. For low strain rates ($<0.02 \text{ s}^{-1}$ for human spinal cord and $<0.01 \text{ s}^{-1}$ for rat spinal cord, respectively), the stress increases almost linearly as the strain is increased, which means that the modulus remains constant. The slope of the stress-strain curve within this linear region is called the pseudo-modulus.

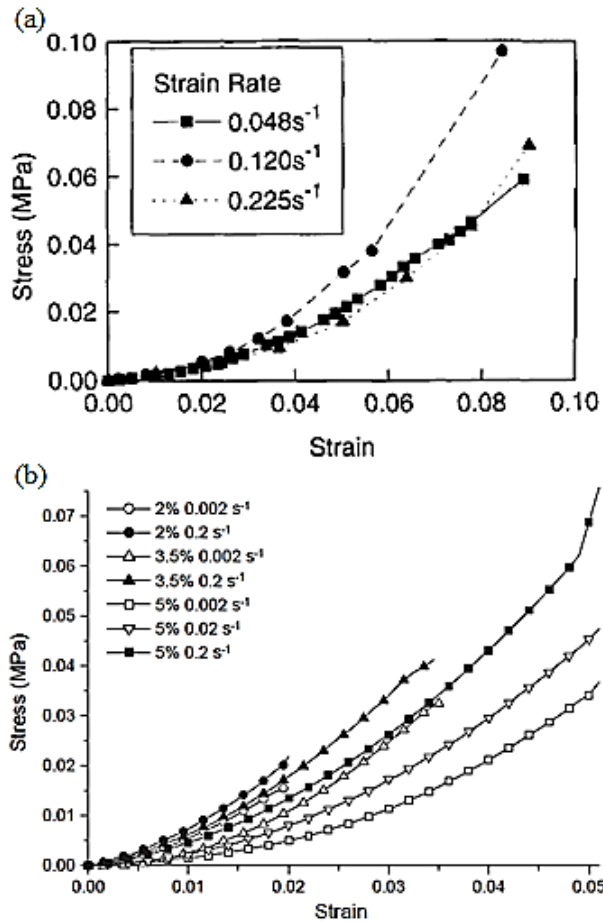


Figure 2-3: Stress-strain curves for (a) human cervical spinal cord [4] and (b) rat spinal cord [5] at different strain rates. The standard deviations were not plotted in this figure for clarity. A non-linear response in which the modulus increases with an increasing of strain can be seen.

2.1.1 Characterization methods

Several researchers have tested the mechanical properties of real spinal cords. The spinal cord is complex and fragile [9, 10]; therefore the testing can be a very delicate process.

Due to the elongated, cylindrical shape of the spinal cord, tensile testing is the most common characterization method used to test the spinal cord [4-8, 10-12]. A typical

testing setup is shown in Figure 2-4 [4]. In this test, the segments to be tested must either be clamped or glued to the force tester. Then, the desired strain rate profiles are applied, and the stress required to maintain the desired rate is measured during the stretching process [4-8, 10-12]. In most spinal cord studies described in the literature, either a constant strain rate is applied, or a range of constant strain rates are applied to investigate the time-dependent rheological properties of the spinal cord.

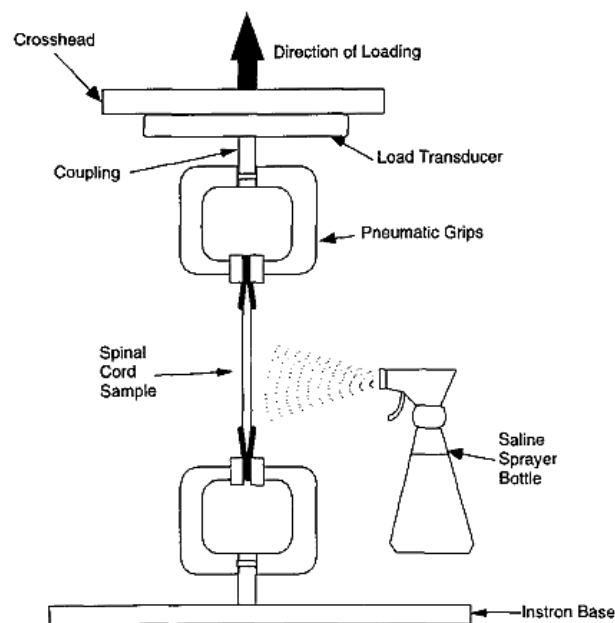


Figure 2-4: A typical tensile testing setup for spinal cord. This setup is used to measure the mechanical properties of human cervical spinal cord *ex vivo*. The samples are fixed with grips at both the ends. The upper grip was attached to a load cell which can apply the loading conditions and record the resultant force data. Saline is sprayed on the sample to prevent it from drying during testing [4].

Tensile testing may be done either *in vivo* [4, 5, 11, 12] or *ex vivo* [6-8]. For *ex vivo* testing, the specimen must be removed from the animal and loaded to the tensile tester

for testing as soon as possible. After death, the properties of spinal cord changes rapidly from those in a living system, whether or not the cord is removed from the spine [7]. There are a number of reasons why this occurs: the spinal cord lacks perfusion after death and/or removal [9]; the tissue may break during removal [11], and the cord dries rapidly when it is removed from its surroundings. Saline can be sprayed on the spinal cord during the tests to prevent it from drying [4, 10, 11], to prevent the mechanical properties from changing.

For *in vivo* tests, only a small specimen need be fixed to the tester, which requires removal of relative smaller range of bones, enabling characterization in living animal specimens. For both *ex vivo* and *in vivo* measurements, preconditioning [4, 11] of the specimens can be used to release some of the stress of the samples which could influence the stress relaxation behavior later [4, 5]. In the pre-conditioning process, the samples undergo cyclic loading conditions similar to the actual testing cycle to remove the previous loading effect.

Due to all of the parameters which can be varied during testing, including strain rate, *in vivo* or *ex vivo* measurements and preconditioning, the mechanical properties of the spinal cord depend strongly on the conditions under which the tests are performed.

The results of various tensile tests from the literature, especially concerning the moduli of different types of spinal cords, will be discussed in later sections. Relevant condition of testing will also be discussed.

2.1.2 Mechanical properties in the literature of animal and human spinal cords

2.1.2.1 Mechanical properties of spinal cords reported in the literature

Ideally, the modulus of our surrogate cords would be similar to that of the human spinal cord *in vivo*. However, it is practically difficult and ethically impossible to measure the modulus of living human spinal cord *in vivo*. The properties of the human spinal cord have, however, been measured *ex vivo* [4, 12].

Bilston *et al.* [4] used uniaxial tensile tests to measure the mechanical properties of human cervical spinal cord with both *pia* and *dura mater* intact. In their research, the cervical human spinal cords were dissected to the right length before testing, and each cord was glued to the clamps of loading cell. During the measurements, the spinal cord was prevented from drying by spraying saline around the sample. The applied strain rates range from 0.04 to 0.24 s⁻¹. The spinal cords exhibited non-linear stress-strain response and the measured values range from 0.9-1.5 MPa under these conditions.

Mazuchowski *et al.* [12] measured the elastic modulus of *ex vivo* human spinal cords both with and without *pia mater*. A picture of a representative human spinal cord is shown in Figure 2-5 [12]. In their research, 18 adult human spinal cords were harvested immediately upon death and kept in 0.9% Sodium Chloride at 4°C to minimize the change in properties. The specimens were tested within 48 hours upon removal. In this experiment, the specimens were stretched until a predetermined stretch ratio, which is defined as the ratio of the final length to the original length. The

measured moduli for human spinal cord with and without *pia mater* were 1.4 MPa and 0.089 MPa, respectively. The value for human spinal cord with *pia mater* was similar to that measured by Bilston *et al.* [4], which verifies this research.

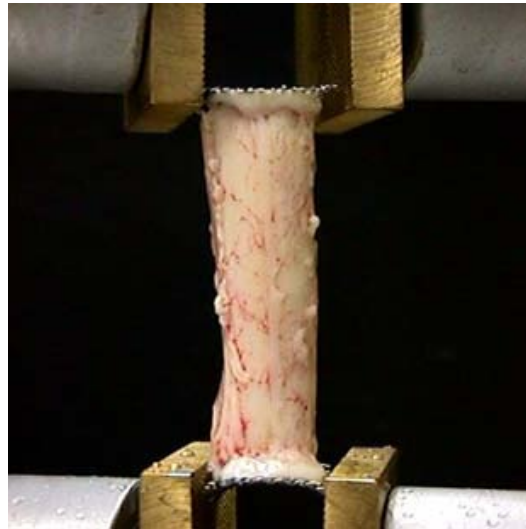


Figure 2-5: Representative human spinal cord specimen [12].

Apart from *ex vivo* human spinal cord, studies have also been taken to measure the animal spinal cords such as cat [7], rat [5], bovine [11] and canine spinal cords [6, 8]. The advantage of animal spinal cord studies is that both *ex vivo* [5, 10, 11] and *in vivo* [6-8] measurements can be taken. These studies also provide valuable resources for the study of mechanical properties of human spinal cord due to the similarities between the cords [13-16]. The results of measurements on human and animal spinal cords and the testing parameters are summarized in Table 2-1. There are some differences even between the same type of animal. These differences arise due to variations in strain rates, clamping, preconditioning, etc. which will be discussed in the next section. For

a review of the mechanical properties spinal cord tissue under different experimental conditions, see [17].

Table 2-1: Spinal cord measurements from the literature

Ref. #	Specimen	With <i>pia</i> or without?	<i>In vivo</i> / <i>ex vivo</i>	Measurement conditions (Strain rate and strain)	Modulus
[12]	Human	1) With <i>pia</i>	<i>Ex vivo</i>	1) $<0.2 \text{ s}^{-1}$, 1 s^{-1} and 10 s^{-1} , to strains of 6% to 20%	1) 1.4MPa
		2) Without <i>pia</i>		2) 0.1 s^{-1} , 1 s^{-1} and 10 s^{-1} to strains of up to 50%	2) 0.089MPa
[4]	Human	With <i>pia</i>	<i>Ex vivo</i>	0.048 s^{-1} , 0.120 s^{-1} , 0.225 s^{-1} , to ~10% strain	$1.23 \pm 0.32 \text{ MPa}$
[7]	Feline	With <i>pia</i>	<i>In vivo</i>	0.003 s^{-1} to 7% and 0.012 s^{-1} from 7% to 11%	0.230 MPa
[5]	Rats	With <i>pia</i>	<i>Ex vivo</i>	0.002 s^{-1} , 0.02 s^{-1} , 0.2 s^{-1} to ~ 5% strain	1.14 to 1.98 MPa ^a
[6]	Canine	With <i>pia</i>	<i>In vivo</i>	0.02mm/sec to < 5% strain	0.265MPa
[8]	Canine	With <i>pia</i>	<i>In vivo</i>	0.003 s^{-1} , to 1.7% strain	0.265 MPa
[11]	Bovine	With <i>pia</i>	<i>Ex vivo</i>	0.002 s^{-1} to ~ 8.5% strain	1.19 MPa
[10]	Bovine	With <i>pia</i>	<i>Ex vivo</i>	0.05 s^{-1} to failure	$0.94 \pm 0.13 \text{ MPa}$ for <i>gray matter</i> 0.66 ± 0.16 for <i>white matter</i>

^aValue measured depends on strain rate employed

2.1.2.2 The influence of measurement conditions on the results

The stress-strain behavior of the tensile measurements for all types of animals discussed above was summarized in Table 2-1 [17]. The results showed general agreements with each other but with some disparities. Both *ex vivo* [4, 5, 10-12] and *in vivo* [6-8] measurements have been reported in the literature. One major difference between *in vivo* and *ex vivo* testing is that for *in vivo* tests, the spinal nerve root is intact while for *ex vivo* tests, it is removed. The presence of the nerve roots may give rise to tethering effects when stretched.

There may be some other reasons for the differences in results observed between different testing conditions. One of them is the clamping conditions or the boundary conditions for the tests. When different clamping techniques are used, differences in measurements can be observed. In Hung and Chang's measurements [6-8], the intact length of the spinal cord was glued to the clamps, while in the more recent measurements, the spinal cords was dissected and then part of the spinal cord was glued to pincer-like clamps [4, 12]. In this set-up, the dissected spinal cord could move and deform partly outside the clamps.

In addition, the pre-conditioning may cause the fiber in the spinal cord to release from twisting somewhat. Longer pre-conditioning circle time and larger pre-strain may results in some "softening effect" of the spinal cord, which causes the modulus to decrease.

Another factor that can affect the measurements is whether or not the *pia mater* and *dura mater* have been removed before characterization. There are three layers surrounding the spinal cord, both protecting the spinal cord and providing the suitable environment for the spinal cord, as we mentioned in Chapter 1. *Pia mater* is the innermost meninges of spinal cord. It is much stiffer than the spinal cord tissue, and protects the spinal cord. There are measurements of spinal cord with *pia* [4-8, 11, 12] and *without pia* [10, 12]. In the measurements of human spinal cord, the spinal cord with *pia* is much stiffer than that without *pia* (1.4 MPa compared to 89 kPa for the human spinal cord, shown in Figure 2-6) [12], indicating that the *pia* contributes most of the stiffness in the measurement. Therefore, it is important to consider whether the target modulus for our surrogate spinal cords should be with *pia* or without.

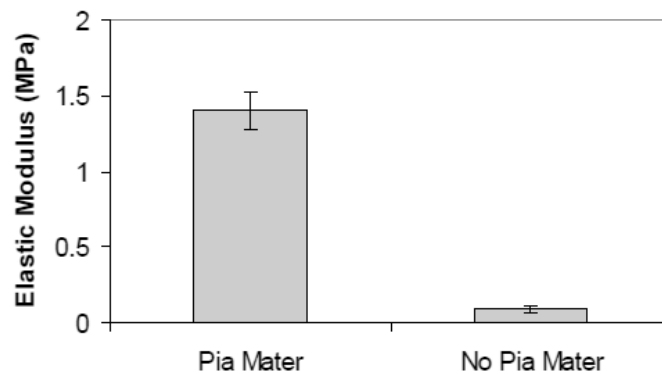


Figure 2-6: Comparisons of *ex vivo* human spinal cord with and without *pia mater* [12].

2.1.3 Target modulus for the surrogate spinal cord

The previous literature on the tensile tests of human and animal spinal cords provides valuable data on identifying a target modulus for our surrogate spinal cord. In this thesis, our objective is to design a surrogate spinal cord that can be used to characterize

the mechanical interactions between the cord and ISMS electrodes. To reach the right locomotor tissue in the *gray matter*, the electrodes would be inserted to a depth of 3-4 mm. However, the thickness of the *pia mater* is only less than three hundred microns thick [18]. Therefore, the majority of the surface of each electrode will be in contact with the spinal cord tissue itself (rather than the *pia mater*), which means that surrogate cord should be designed to mimic the modulus of human spinal cord without *pia mater*. Based on the above discussions, our target modulus is chosen to be 89 kPa.

2.2 Previous research on the surrogate spinal cords

Several surrogate spinal cords which mimic the mechanical properties of real spinal cords have been reported in the literature. In this section, previous surrogate spinal cords described in the literature will be discussed, and the main classes of materials commonly used to build surrogate spinal cord will be introduced. Among the materials used in the literature, silicone elastomers [19-22] and uncrosslinked gelatin [23] are the most common, and both of these classes of materials will be considered as candidate materials in the research described in this thesis. As will be described, most of the previous work has been aimed at developing models to test injury mechanisms, and therefore the requirements of these systems differ somewhat from surrogate cords developed to test electrode stability.

2.2.1 Surrogate cords made by silicone elastomers

Silicone elastomers are a class of polymers containing silicon, carbon, hydrogen and oxygen. Instead of having a C-O-C or C-C-C backbone in their structure after curing (as for most polymers), silicone elastomers have a Si-O-Si backbone (polysiloxane) (shown in Figure 2-7), which contributes to its unique mechanical properties. The structure of polysiloxane is very flexible because the bond lengths and bond angles between Si-O-Si are large compared to many other structures, such as C-C and C-O-C backbones. This means that polymers with Si-O-Si backbones can undergo more movement under deformation. Therefore, the moduli of silicones are very low (ranging from about 0.1MPa [24] to 10 MPa [25]).

Many types of silicone elastomers can be prepared by mixing two components (an elastomer base and a crosslinker) together and curing them under a certain heating curve. The micro-structure of the elastomer base is linear, resulting in weak bonding between chains. The crosslinking reaction bonds the polymer chains together, resulting in network structure, which stabilizes and hardens the silicone. The ratio of elastomer base: crosslinker determines the extent of crosslinking. Larger crosslinker content causes the silicone to be more stable and stiff due to the large portion of network-like bonds. Therefore the mechanical properties of silicone elastomers are dependent on the ratio of elastomer:crosslinker.

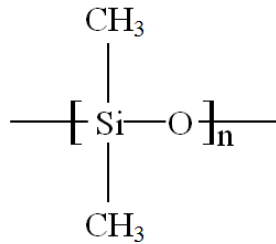


Figure 2-7: The general structure of silicone elastomer monomer.

Another important property of silicones is that they are very stable and inert to most organic and inorganic chemicals due to the high strength of the silicon-oxygen bond. Due to their softness and stability, silicones have been used in biomaterials engineering, electrical engineering and food sciences. Typical applications of silicone include skin substitutes (Figure 2-8) [26], drug delivery [27] and nanotechnology [27]. The above properties of silicone elastomers made them promising candidate to mimic the mechanical properties of spinal cord soft tissue. Silicone elastomers are the most common type of material used in the fabrication of surrogate spinal cord in previous studies [19-22]. In many of these previous studies [21, 22], the elastomer:crosslinker ratios were varied to try to match the mechanical properties of real spinal cords. Three studies to construct surrogate spinal cords with silicone elastomers will be described in this section.

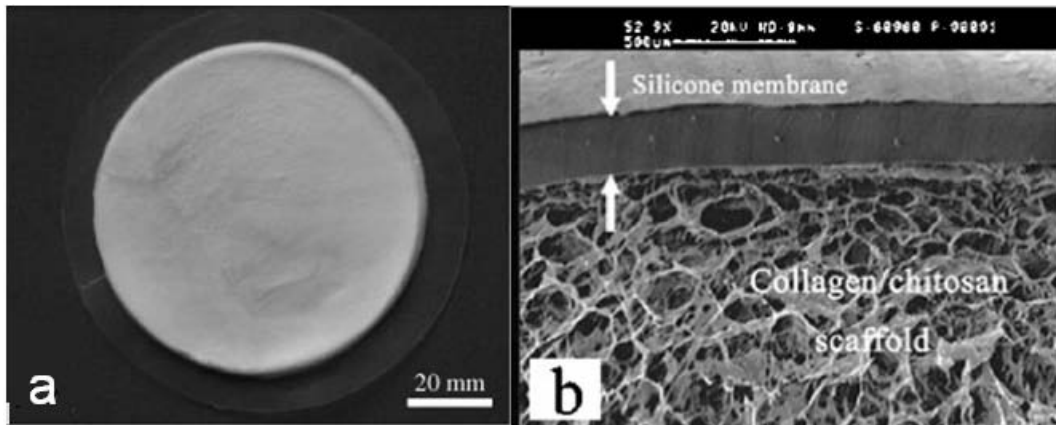


Figure 2-8: Example of the applications of silicone elastomers as skin substitute in biomaterials engineering: a) Picture of the bilayer; (b) The microstructures of the bilayer imaged by scanning electron microscope. Silicone membrane was attached to collagen/chitosan scaffold to provide suitable water permeability to mimic that of the skin [26].

To engineer a system to simulate the extent of deformation of human spinal cord during hyperextension or hyperflexion injury, Bilston *et al.* [19, 20] built a surrogate cord with Sylgard 527 obtained from Dow Corning Ltd. (Midland, Michigan, USA) to match the mechanical properties of human spinal cord *ex vivo* in tension. This surrogate cord was placed in the vertebral canal of a plastic spinal cord. The model was then subject to a loading condition to simulate the process of spinal cord injury. The measured axial compressive strain was between 0 % and 15 % in these experiments.

Kroeker *et al.* [21] designed an improved surrogate spinal cord model which mimics both the tensile and bulk compressive moduli of *ex vivo* human spinal cord. In their research, the quasistatic tensile properties of 6 types of silicones, including Sylgard 527 were measured. Both Sylgard 527 and another type of silicone, QM Skin 30, were

each mixed at different ratios of elastomer:crosslinking agent to vary the tensile modulus. It was found that the QM Skin 30 at a mixing ratio of 10:1.2 had the closest quasistatic tensile behavior to that of the human spinal cord *ex vivo*, and this material was chosen to build their surrogate cord. In subsequent tensile and compressive tests, this surrogate cord was proved to simulate both the tensile modulus and the bulk compressive modulus of the human spinal cord (shown in Figure 2-9).

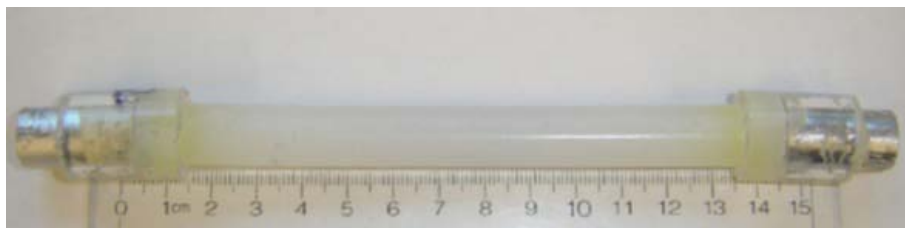


Figure 2-9: Surrogate spinal cord made by QM Skin 30. Both of the ends of surrogate cord were glued by epoxy to facilitate the clamping in the subsequent mechanical tests [21].

Jones *et al.* [22] also used a QM Skin 30 surrogate cord to evaluate the effect of cerebrospinal fluid (CSF) on spinal cord deformation. Instead of real CSF, saline – which was referred to as “pseudo-CSF” – was used as a substitute because of its similarity in both rheological properties and chemical composition. Three configurations of surrogate cords were characterized: (1) QM Skin 30 surrounded with pseudo-CSF, surrounded by bovine *dura mater*, (2) QM Skin 30 encased in bovine *dura mater* without pseudo-CSF, and (3) neat QM Skin 30 without either *dura* or pseudo-CSF. These combinations were examined under burst fracture simulation apparatus which mimics the loading condition of human bone fracture. To verify that surrogate cord can mimic burst fracture, the deformation of bovine spinal cord under

the same loading conditions were also examined. It was shown that CSF acts as a protective agent during deformation, reducing the amount of deformation in each cord and extending the time of deformation before failure.

2.2.2 Surrogate cords made by gelatin

Gelatin is a biocompatible and tasteless material derived from collagen, which is a type of protein found in animal skin and bones. It is produced by irreversibly hydrolyzing collagen. There are 18 distinct amino acids found in different types of gelatin, all of whose structures are left-handed helices. Of these amino acids, one fourth is various basic amino acids; one third are glycine (Gly) and one third are proline or hydroxyproline (Pro). The basic unit in gelatin is:

Gly-Pro-X

Where X is acidic or basic amino, often hydroxyproline. The molecular structure of proline and glycine are shown in Figure 2-10.

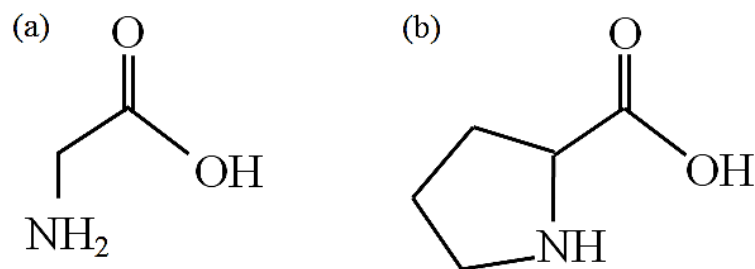


Figure 2-10: Molecular structure of (a) proline and (b) glycine.

The raw material of gelatin is supplied in powder form. Generally, two distinct types of sample can be made from gelatin, gelatin hydrogels (which contain high levels of water) and dry gelatin hard films. The mechanical properties of the hydrogel form of gelatin and dry gelatin are quite different. Gelatin hydrogels are very soft, and their mechanical properties are dependent on the water content of the sample [23, 28, 29]. The elastic shear modulus of hydrated gelatin can be as low as 1.16 kPa [29]. Dry gelatin samples can be very hard, having elastic moduli in the range of 3.6-12.0 GPa measured in tensile tests [28, 30, 31].

The bonds between adjacent chains for uncrosslinked gelatin are weak. To increase the stability of this material, crosslinkers such as formaldehyde [32], glutaraldehyde [33], glyoxal [32] and genipin [34] can be added to react with active amino and hydrogen groups on the gelatin. Apart from these chemical crosslinking methods, there are also physical crosslinking methods such as UV exposure [35]. The mechanical properties and biocompatibility of gelatin make it ideal candidate for drug delivery [36, 37], 3D scaffolds [38] and other biomaterials applications such as bioadhesives. Typical applications of gelatin in biomaterials are shown in Figure 2-11.

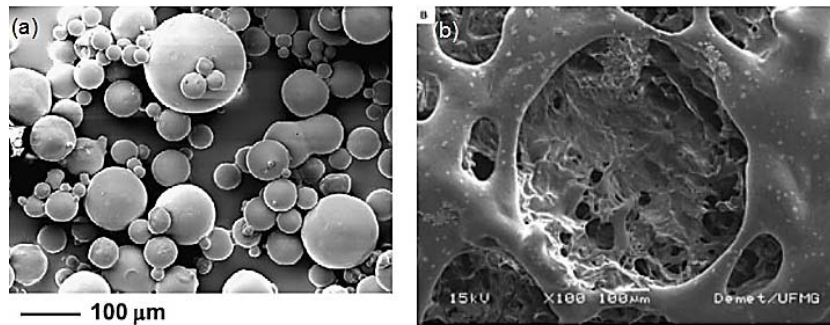


Figure 2-11: Scanning electron micrographs of (a) gelatin microspheres for drug delivery [37]

(b) Cross-sectional of a 3D chitosan–gelatin–chondroitin scaffold [38].

The softness of gelatin also makes it ideal candidate material for use in surrogate spinal cords. Pintar *et al.* [23] developed a surrogate cord consisting of a collagen casing with an uncrosslinked gelatin filling. To find the right ratio of gelatin:water for the surrogate cord, the compressive behavior of different gelatin samples in collagen casings were compared to that of the feline spinal cord. The compressive behaviors of feline spinal cord and uncrosslinked gelatin were measured by dropping a fixed mass from a fixed height. An apparatus was used to measure and record the acceleration and displacement. It was found that the 2.9 wt% uncrosslinked gelatin had the closest stress-strain response to that of the feline spinal cords (as shown in Figure 2-12). After the surrogate cord with the right weight percent was produced, the cord was then placed in the spinal canal of a human cadaveric head-neck complex and underwent a loading which could cause bone fracture. The transverse pressure experienced in the cord during the process was measured by transducers embedded in the cord, and it was found that the highest pressure occurred near the location of fracture. This study contributed to the knowledge of the biomechanics of spinal fracture and dislocation.

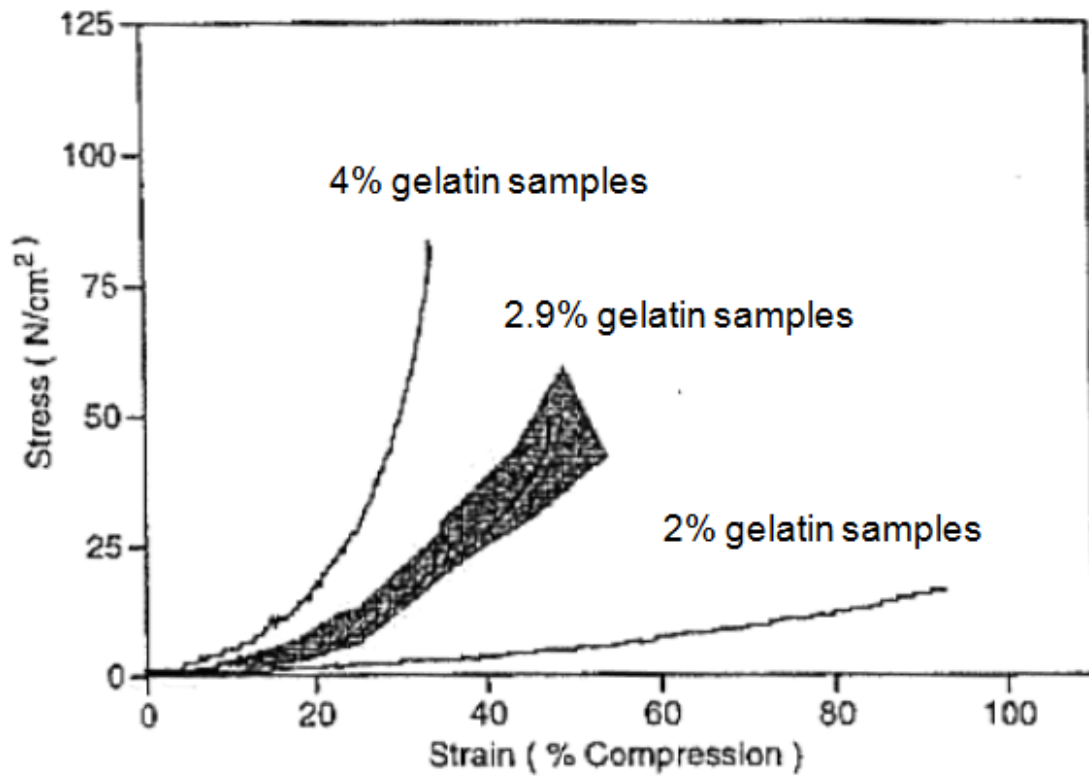


Figure 2-12: The comparison of the stress-strain behavior of different wt% gelatin samples and the feline spinal cords (the shaded area) under compression. It was found that the 2.9 wt% gelatin has the closest compression behavior of feline spinal cord which lined in the middle of the shaded area. Adapted from [23].

2.2.3 Shortcomings of the previous surrogate spinal cords

Previous surrogate spinal cords provide a valuable starting point for the selection of candidate materials for use in the surrogate spinal cords described in this thesis, and a summary of these cords is shown in Table 2-2. In my study, both the silicone elastomers and hydrated gelatin will be considered as candidate materials. Various materials will be tested in various concentrations and various mixing ratios. To

improve the stability of uncrosslinked gelatin (which is fragile and difficult to handle), it will be chemically crosslinked in my work.

The previous surrogate spinal cord studies also provided some of the testing protocols for characterizing the candidate materials. Matching the elastic modulus of real spinal cord tissue is of great importance when selecting a material from which to construct surrogate cords. Therefore, tensile tests will be used to measure the tensile moduli of each candidate material, and these values will be compared to the target modulus (89 kPa) discussed earlier in this chapter.

A major difference between the work described here and the work described previously in the literature is that the main objective of the previous studies was to develop surrogate spinal cords to study the injury mechanisms of the spinal cord. Therefore, only the elastic moduli of candidate materials were tailored to mimic real spinal cords. For my work evaluating the mechanical of implanted neural prostheses, the surface properties of the surrogate material must also be carefully considered, since this property influences the behavior during the insertion of the electrodes, and also affects the relative movements that take place between the cord and the electrode arrays during the natural motion of the spinal cord. Therefore, the surface properties of the candidate materials must be matched to those of real spinal cords. In subsequent chapters, the mechanical and surface properties of the candidate materials described above will be used to choose the material most suitable for use in a surrogate spinal cord for the testing of ISMS electrode arrays.

Table 2-2: Summary of the previous surrogate spinal cords

Ref. #	Purpose	Target properties	Characterization method	Materials
[19, 20]	Measure the extent of deformation of spinal cord when SCI occurred	Tensile modulus of human spinal cord <i>in vitro</i>	Tensile testing	Sylgard 527
[21]	Improve extent of similarities of surrogate cord	Tensile and bulk compressive moduli of human spinal cord <i>in vitro</i>	Tensile and compressive testing	QM Skin 30
[22]	Evaluate the effect of CSF to the extent of deformation	Deformation behavior of bovine spinal cords with both <i>dura</i> and CSF, with only <i>dura</i> and without <i>dura</i>	Tensile testing mimics burst fracture	QM Skin 30
[23]	Measure the pressure profile during spinal fracture	Compressive stress-strain behavior of feline spinal cords	Drop mass test	Uncross -linked gelatin

Chapter 3* Materials selection

Once an electrode array is implanted in the spinal cord for ISMS, it would ideally function for the lifetime of the patient. Therefore it is crucial to ensure that the electrode arrays do not cause damage to the delicate spinal cord during the natural motion of spinal cord. To facilitate testing in lab, the motivation of this research is to test the long-term mechanical stability and interactions of both existing and proposed electrode arrays with a proof-of-concept physical spinal cord model (i.e., the surrogate spinal cord). The surrogate cord must simulate the mechanical properties of the spinal cord. The surface properties of the candidate materials must also be considered, since frictional force at the surface of the cord plays a role both as the electrodes are inserted, and as the spinal cord deforms.

In this study, three characterization methods were used to evaluate the properties of the candidate materials, which were compared to those of the real spinal cords. For mechanical properties, Dynamic Mechanical Analysis (DMA) was used measure the elastic modulus of the candidate materials. The results were compared to the modulus of the human spinal cord *ex vivo* without *pia mater* described in the literature, as was discussed in Chapter 2. Indentation testing was used to evaluate the force required to achieve specified displacements, which represents the compressive modulus in surrogate cords made from candidate materials, as well as in actual rat spinal cords.

* Parts of this chapter have been submitted for publication in the *Annals of Biomedical Engineering* (November 11, 2011)

The surface properties of the candidate materials and rat spinal cords were measured by pulling a needle out of each material at a controlled rate, and measuring the pulling force.

In this chapter, the characterization of two classes of materials, silicone elastomers and gelatin hydrogels will be described, and the materials with the properties that best mimics those of actual spinal cords will be selected from which to construct surrogate spinal cords.

Three types of real spinal cords were involved in this study. The surrogate spinal cord was molded based on the dimension of feline spinal cord obtained from MRI image.

The modulus of human cervical spinal cord measured *ex vivo* (89 kPa) was used as the target modulus in the DMA tensile measurements. Finally rat spinal cords were harvested and tested immediately in the indentation tests and frictional tests. The reason for choosing the dimension of feline spinal cord is that the preliminary ISMS tests will be carried out on cats by my co-workers. Therefore it is desirable to test the mechanical stability of electrode arrays implanted in surrogate cords with dimensions based on feline spinal cords. Once the arrays are tested in the feline model, it will be desirable to modify the design for use in humans. The modulus of human spinal cords is therefore considered. The reason for choosing fresh rat spinal cord for direct comparison in some of our tests is that it is unfeasible to obtain either fresh human or feline spinal cords in the lab due to large cost of harvesting feline spinal cords.

Therefore rat spinal cords are the most efficient model for *ex vivo* characterization. In terms of mechanical properties of human and rat spinal cords, similarities in the tensile mechanical behavior between human and rat spinal cords *ex vivo* were found. Bilston *et al* [1]. measured the tensile properties of human cervical spinal cord *ex vivo* with *pia mater* intact at a strain rate of 0.225s^{-1} to about 10% strain for each sample tested, and observed a tensile modulus of 1.23 ± 0.32 MPa. For rat spinal cords, the measured modulus by Fiford *et al.* [2]. was about 1.14MPa at strain rate of 0.2 s^{-1} which was very close to the strain rate applied in Bilston's research. In addition, the motor neuron distribution within the ventral horn of rats is very similar to humans [3-6]. Based on the above discussions, the use of rat spinal cord for direct comparison of the indentation behavior to those of the candidate material is reasonable.

3.1 Candidate materials and sample preparation

Based on the discussions in Chapter 2, silicone elastomers and gelatin hydrogel were chosen as candidate materials.

Sylgard 184 was obtained from Dow Corning Ltd. (Midland, Michigan, USA) as a two component system (elastomer and crosslinker), and was prepared by mixing the two components in ratios of elastomer:crosslinker of 10:1, 20:1, 30:1, 40:1 by weight.

Samples were crosslinked by baking at 60°C for 3 hours. QM Skin 30 was obtained from Quantum Silicones LLC (Richmond, Virginia, USA), and was prepared by mixing the two components in a ratio of 10:1 (as directed) and curing these samples for 24 hours at room temperature. TCB 5101 was obtained from BJB Enterprises, Inc.

(Tustin, California, USA), and samples were prepared by mixing the two components in a 1:1 ratio (as directed) and curing the mixture in an appropriate mold (as described below) for 24 hours at room temperature.

Gelatin powder was obtained from Sigma Aldrich (G1890, gelatin from porcine skin, Oakville, Ontario, Canada), and was used as received. To prepare the uncrosslinked 9 wt%, 12 wt% and 15 wt% gelatin in water, a suitable mass of powder was dissolved in distilled water. Solutions were then heated to 55°C and stirred at a rate of 60 revs/min for 20 minutes. The solutions were then poured into a mold, and allowed to set overnight in the refrigerator. The uncrosslinked gelatin was fragile and difficult to handle; therefore, formaldehyde (19.4 mmol/100ml) was employed as a chemical crosslinker to increase the stability and handleability of the samples, as described by de Carvalho *et al.* [7]. After a solution of gelatin was prepared and stirred as described above, formaldehyde was added, and the solution was stirred for an additional 15 minutes at 45°C. This solution was then set in the refrigerator overnight in a suitable mold.

Flat samples for measurements of modulus of elasticity were polymerized in 90 mm × 90 mm polystyrene weighing boats, and surrogate cords with elliptical cross-sections were prepared using an aluminum mold, as described in section 3.2.

3.2 Construction of surrogate spinal cord

Surrogate cords with elliptical cross-sections (6 mm × 8 mm) were prepared by curing silicones or gelatin in a custom-made aluminum mold (shown in Figure 3-1). The

dimensions of the elliptical cross-section of the mold were based on magnetic resonance images (MRIs) of lumbosacral regions of the cat spinal cord (shown in Figure 3-2, taken by Vivian Mushahwar, Department of Cell Biology, University of Alberta). The length of each as-molded cord was 7 cm, although the cords could be cut to a desired length. As described above, the dimensions of the cat (rather than human) spinal cord were chosen because the cat is used as the primary model for intraspinal microstimulation implants [3, 8-10]. Therefore, the mechanical interactions of implants and the surrogate cords can be compared to histological and electrophysiological results obtained in this animal in the future. Samples were typically cured overnight in the mold (wrapped in plastic to minimize drying), and characterized the following day. When preparing silicone cords, the mold was pre-coated with vacuum grease (Dow Corning, High Vacuum Grease, Midland, MI) to prevent the silicones from bonding to the surface of the mold. A representative picture of the surrogate spinal cord made by gelatin hydrogel is shown in Figure 3-3.

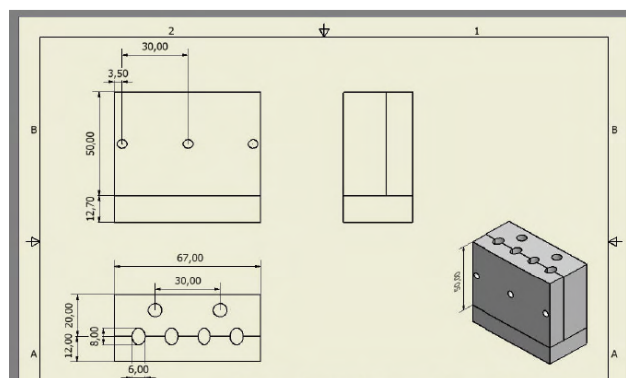


Figure 3-1: Schematic for the aluminum mold for producing the surrogate spinal cords with its dimensions. The cords were molded by pouring the candidate materials into the 4 holes seen on top of the mold in the diagram.

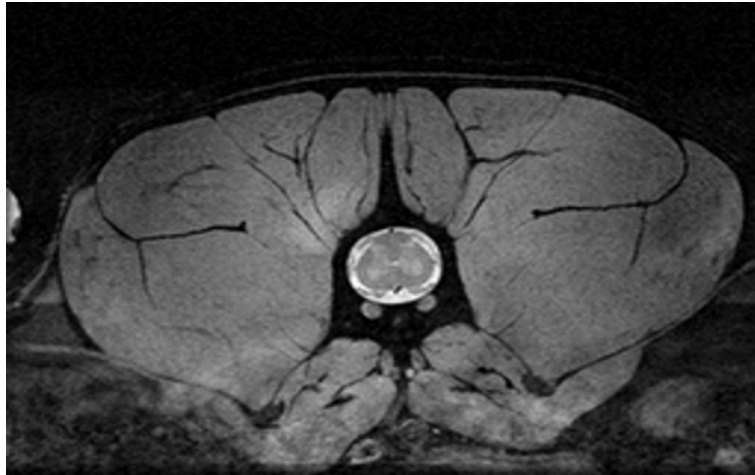


Figure 3-2: MRI image of feline spinal cord. (Provided by Vivian Mushahwar, Department of Cell Biology, University of Alberta).

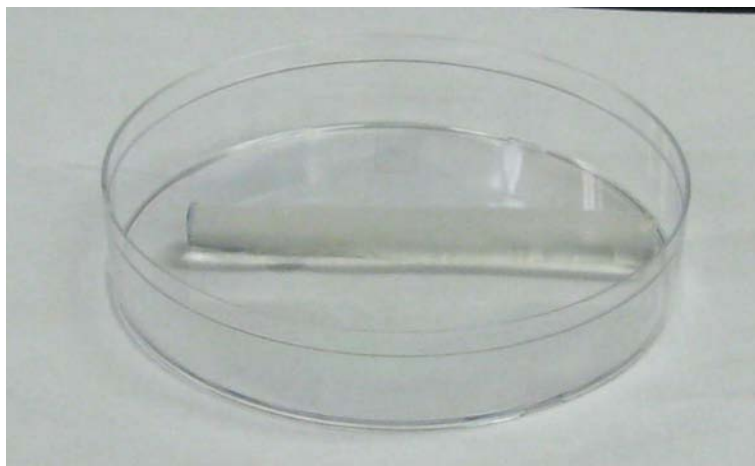


Figure 3-3: Representative image of a surrogate spinal cord in a petri dish.

3.3 Characterization of surrogate spinal cord materials

3.3.1 Dynamic Mechanical Analysis (DMA)

Dynamic Mechanical Analysis (DMA) is a characterization technique for measuring the mechanical and thermal properties of materials, especially the viscoelastic behavior of polymers. In DMA measurements, the sinusoidal stress profile required to deform

a sample with a controlled degree of sinusoidal strain is measured. In my work, the DMA 8000 (Perkin Elmer, Waltham, Massachusetts, USA, shown in Figure 3-4) is used to measure the tensile modulus of the candidate materials. For each candidate materials, the tensile storage modulus is measured and compared to that of the target modulus (89 kPa) [3, 11].

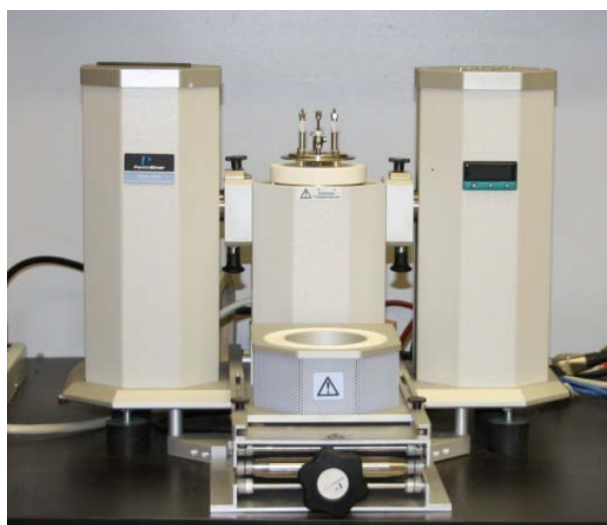


Figure 3-4: Picture of DMA 8000.

Samples were characterized using the tension fixtures for the apparatus. In this geometry, a sample with a rectangular cross-section is required in order to achieve the most accurate measurements. Flat, hydrated gelatin samples were cut into dimension of approximately $11 \text{ mm} \times 7.5 \text{ mm} \times 3.5 \text{ mm}$ (length \times width \times thickness), and silicone samples were cut to have dimensions of approximately $13 \text{ mm} \times 7 \text{ mm} \times 2 \text{ mm}$. Samples were loaded into the DMA using the appropriate clamps; after clamping, a typical sample length was $\sim 6 \text{ mm}$. All tests were taken at room temperature (in the range of 21.7°C to 25.5°C) for comparison with other results from the literature.

During characterization, the displacement and frequency of the strain were controlled to 0.01 mm and 1 Hz respectively, to minimize the viscous component of the response. For each material, a minimum of 3 different samples were measured, and each sample was characterized 3 times. Statistical analysis could then be performed on the results to determine which materials had moduli which were similar to the target modulus (within the range of uncertainty obtained in the measurements).

The differences between the mean value of each candidate material measured by DMA measurements (x_{ave}) and the target modulus from the literature ($x_{target} = 89$ kPa) was compared using the standard deviation (σ) of the modulus for each candidate material:

$$t = |x_{ave} - x_{target}| / \sigma \quad (3.1)$$

The calculated value t represents the discrepancy. If t is less than 1.96, then the modulus of this material is considered to be acceptably close to the target modulus. If t is larger than 1.96, the measured modulus is considered significantly different from the target modulus.

For the Sylgard 184 silicones, the mechanical properties are dependent on the ratio of base:crosslinker. Samples made using 4 different mixing ratios were measured, and the results were shown in Table 3-1 and plotted in Figure 3-5. The moduli of Sylgard 184 in crosslinking ratio of 10:1, 20:1 and 30:1 were much higher than that of the target modulus (89 kPa [11]), and all values were significantly different from the target modulus ($t > 1.96$). The value of 40:1 Sylgard 184 was the closest to the target modulus,

although the discrepancy between the values varied by 2.2 times the uncertainty in the measurement, and is therefore considered to be significantly different.

Table 3-1: Average tensile moduli and standard deviations of Sylgard 184 at mixing ratios (elastomer: crosslinker) of 10:1, 20:1, 30:1 and 40:1.

Ratio of elastomer :crosslinker	Average tensile modulus/ kPa	Standard Deviation/ kPa
10:1	1829.0	61.5
20:1	901.3	74.1
30:1	352.5	35.0
40:1	147.6	26.8

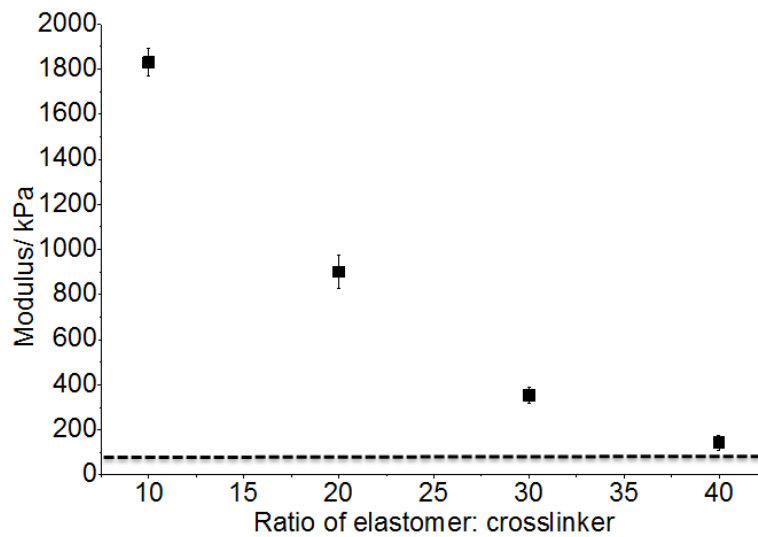


Figure 3-5: Tensile moduli of Sylgard 184 at mixing ratios (elastomer: crosslinker) of 10:1, 20:1, 30:1 and 40:1. The target modulus (89 kPa) was plotted in the horizontal dashed line for comparisons. Average value and standard deviation are shown, based on a minimum of 3

different samples, each of which was tested 3 times.

The tensile moduli of 40:1 Sylgard 184, TCB 5101 and QM Skin 30 are shown in Table 3-2 and plotted in Figure 3-6. The modulus of each material was significantly higher than the target modulus ($t > 1.96$).

Table 3-2: Average tensile moduli and standard deviations of 40:1 Sylgard 184, TCB 5101 and QM Skin 30.

Material	Average tensile modulus/ kPa	Standard Deviation/ kPa
40:1 Sylgard 184	147.6	26.8
TCB 5101	177.9	32.2
QM Skin 30	217.9	44.2

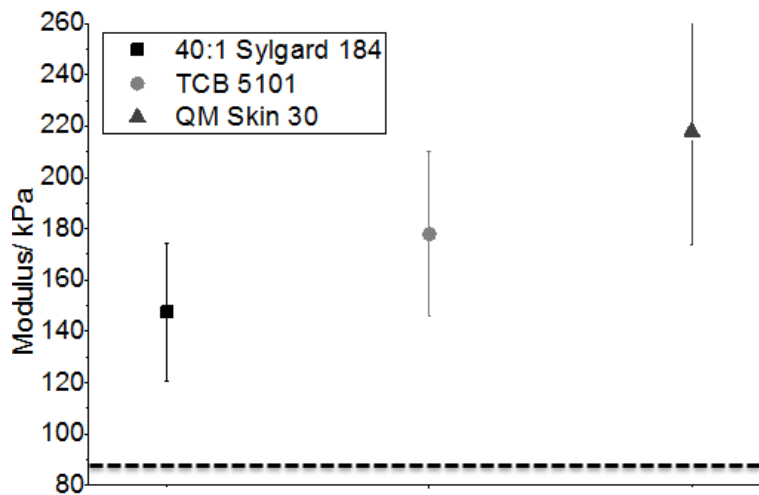


Figure 3-6: Tensile moduli of 40:1 Sylgard 184, TCB 5101 and QM Skin 30. The target modulus, 89kPa was plotted in horizontal dashed line for comparisons. Average value and standard deviation are shown, based on a minimum of 3 different samples, each of which was tested 3 times.

To verify the measurements by DMA, the results of the 10:1 Sylgard 184 (recommended by the manufacturer) of this research were compared to those from the literature. The tensile modulus of the 10:1 Sylgard 184 measured here was 1828 ± 61.5 kPa, which was similar to the value obtained by White *et al.* (1.4 MPa, measured from 10 to 100 Hz) [12] and by Brown *et al.* (1783 ± 177 kPa) [13]. The tensile modulus of QM Skin 30 was 217.9 ± 44.2 MPa, which was slightly higher than the values obtained by Kroeker *et al.* (185 ± 30 MPa) [14]. In their measurements, the elastic modulus was obtained by stretching the silicones at extremely low strain rates (0.0025 s^{-1}) to yield the quasistatic modulus while in my study; the samples were measured under sinusoidal loading at a frequency of 1 s^{-1} .

The tensile moduli of both uncrosslinked and formaldehyde crosslinked 9 wt%, 12 wt%, 15 wt% gelatin in water samples are shown in Table 3-3 and plotted in Figure 3-7.

The modulus of the uncrosslinked 9 wt% gelatin in water was not included since it is lower than the lower limit that could be measured accurately in tension fixture by DMA (< 40 kPa). As expected, each uncrosslinked gelatin samples had consistently lower moduli than the crosslinked samples at the same concentration. The formaldehyde crosslinked 15 wt% gelatin in water had the closest modulus ($79.6 \text{ kPa} \pm 11.7 \text{ kPa}$) to that of the target modulus ($t = 0.8$), while the modulus of the crosslinked 12 wt% in water is also close ($65 \text{ kPa} \pm 6 \text{ kPa}$), although significantly different ($t = 3.7$). The modulus of the 15 wt% gelatin is therefore not significantly different from the target modulus.

Table 3-3: Tensile moduli of uncrosslinked and formaldehyde crosslinked 9 wt%, 12 wt% and 15 wt% gelatin in water.

Weight percent of gelatin in water/%	Uncrosslinked hydrated gelatin		Crosslinked hydrated gelatin	
	Average modulus/ kPa	Standard deviations/ kPa	Average modulus/ kPa	Standard deviation / kPa
9	N/A	N/A	44.6	8.1
12	51.9	4.8	65.3	6.3
15	73.9	5.9	79.6	11.7

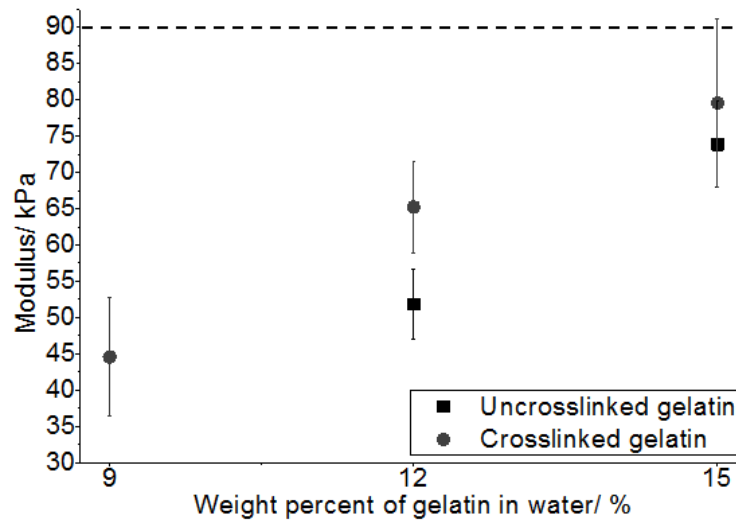


Figure 3-7: Tensile moduli of uncrosslinked and formaldehyde crosslinked gelatins with 9 wt%, 12 wt% and 15 wt% gelatin in water. The target modulus, 89 kPa was plotted as a horizontal dashed line for comparison. Average values and standard deviations are shown, based on at least 4 different samples of each material, each of which was tested at least 3 times.

In our results, the moduli of gelatin were much closer to the target modulus than those of the silicone elastomers, especially for the formaldehyde crosslinked 12 wt% and 15 wt% gelatin in water samples. Small disparities between the measured values and the

target modulus should not be considered significant, due to differences in testing set-up and loading conditions. In the paper from which the target modulus was taken, the measurements were taken using static stress-strain testing for three times at strain rates of 0.1 s^{-1} , 1 s^{-1} and 10 s^{-1} , respectively, while in my measurements a sinusoidal loading cycle to 0.01 mm strain was applied. In addition, differences in the sample shape could also be a factor. In the reference, real human spinal cords with lengths of approximately 5 cm were tested by gluing the ends to the loading cells and applying a very large stretch ratio (1.5). Therefore the cross-section of the testing part would decrease during the stretch, while the ends of spinal cord would remain the same, resulting in non-uniformity in the cross-sectional area tested. In my measurements, rectangular samples were clamped carefully to the machine and relatively low strains (0.01 mm) were applied, preventing the cross-section from changing during the experiments. Based on the above discussions, small variations in the measurements are acceptable. Therefore it could be concluded that the formaldehyde crosslinked 12 wt% or 15 wt% gelatin hydrogel in water or possibly the 40:1 Sylgard 184 could be used to simulate human spinal cord tissue.

3.3.2 The indentation tests

Measurements of modulus of elasticity of spinal cord *ex vivo* are not easily achieved using the DMA method described above, due to the difficulty of clamping the elliptically-shaped spinal cord in a tension fixture. To conduct a direct comparison between the mechanical properties of surrogate materials and real, *ex vivo* spinal cords

under identical conditions, indentation testing was used. Measurements were obtained from rat cords with *pia mater* intact, harvested by our by co-workers in Cell Biology. Surrogate cords were prepared from each material using the aluminum mold, as described in section 3.2, which has cross-sectional dimensions corresponding to those of the cat lumbosacral spinal cord. The difference in the cross-sectional dimensions of cat and rat spinal cords (6 mm × 8 mm and 2 mm × 3 mm, respectively) is not expected to significantly affect the outcome of the indentation tests, which are conducted to a maximum depth of 1 mm.

The indentation test set-up is shown in Figure 3-8. The main part of the set-up is an indenting arm comprised of a cono-spherical tip with a diameter of 1.7 mm. A micrometer was connected to the indenting arm to control and adjust the height of the indenter.

The indentation depth for all the samples was chosen to be 1 mm due to the small cross-sectional dimension of rat spinal cord (approximately 2 mm×3 mm). The softness of the all the materials tested and the shallow indentation depth results in very low indentation force. To ensure accurate measurements, a force transducer and amplifier were used to amplify the force signals. One end of the force transducer was connected to the indenter, and the other was connected to the amplifier. Since the output of the amplifier is in volts, the system had to be calibrated to convert the values to Newtons. A scale was used for the calibration. Before calibration, the indenter was moved downwards until it was just in contact with the scale. The tip of the

indenter was then move downwards in 0.25 mm increments until the depth reached 1 mm. Both the voltage reading from the amplifier and the weight reading from the scale were recorded and compared at the same displacement. It was observed that there was a linear relationship between the two readings, which could be fitted using the equation ($N=m[V]+b$). Once the equation was determined, it could be used to convert a reading in Volts to Newtons.

At least two cords of each material and three rat spinal cords were tested. The testing was repeated at three different spots for each cord (one at each end, and in the middle). Gelatin cords were sealed in plastic during testing to reduce drying, although a small hole was cut through which the tip could access the cord. Prior to each test, the indenter was lowered until the tip was just in contact with the top surface of the cord, and the force transducer was set to 0 N. For each indentation, the tip was displaced at increments of 0.05 mm for the first 0.5 mm, and then at increments of 0.1 mm until the indenting depth reached 1 mm and the force was recorded. The slope of each curve was calculated using linear regression for subsequent analysis.



Figure 3-8: Photos of the setup for indentation test.

The force vs. displacement data measured from at least two different spots for each cord were averaged and shown in Table 3-4 (with standard deviations). The average force vs. displacement curves for surrogate cords made by silicones were plotted in Figure 3-9, and compared to those of the rat spinal cords (data provided by student Jonn Kmech).

Table 3-4: Raw force vs. displacement data for the spinal indentation experiments for silicone cords and the rat spinal cords. We tested 2 cords of each material. Each cord was tested at 3 different positions except in the case of the rat data with 3 cords tested and one of them only tested at 2 positions and two of them at three positions. The averages and standard deviations at each displacement were calculated.

Displacement (mm)	QM Skin 30		40: 1 Sylgard		TCB 5101		Rat spinal cord	
	Average force/N	St. Dev /N						
0	0	0	0	0	0	0	0	0
0.05	0.008	0.003	0.007	0.003	0.008	0.004	0.004	0.003
0.1	0.013	0.005	0.011	0.004	0.011	0.005	0.004	0.003
0.15	0.021	0.007	0.016	0.007	0.016	0.006	0.005	0.004
0.2	0.028	0.009	0.023	0.011	0.02	0.006	0.006	0.004
0.25	0.036	0.014	0.028	0.014	0.025	0.007	0.007	0.005
0.3	0.044	0.017	0.034	0.018	0.029	0.009	0.011	0.005
0.35	0.054	0.021	0.04	0.023	0.034	0.010	0.012	0.006
0.4	0.063	0.025	0.047	0.026	0.039	0.011	0.014	0.006
0.45	0.072	0.028	0.053	0.030	0.045	0.012	0.017	0.006
0.5	0.082	0.031	0.06	0.035	0.051	0.013	0.021	0.007
0.6	0.103	0.038	0.076	0.045	0.064	0.016	0.022	0.009
0.7	0.126	0.043	0.089	0.054	0.074	0.018	0.023	0.009
0.8	0.149	0.048	0.103	0.064	0.086	0.021	0.029	0.012
0.9	0.173	0.051	0.117	0.074	0.099	0.024	0.035	0.013
1	0.195	0.056	0.131	0.083	0.113	0.025	0.04	0.016

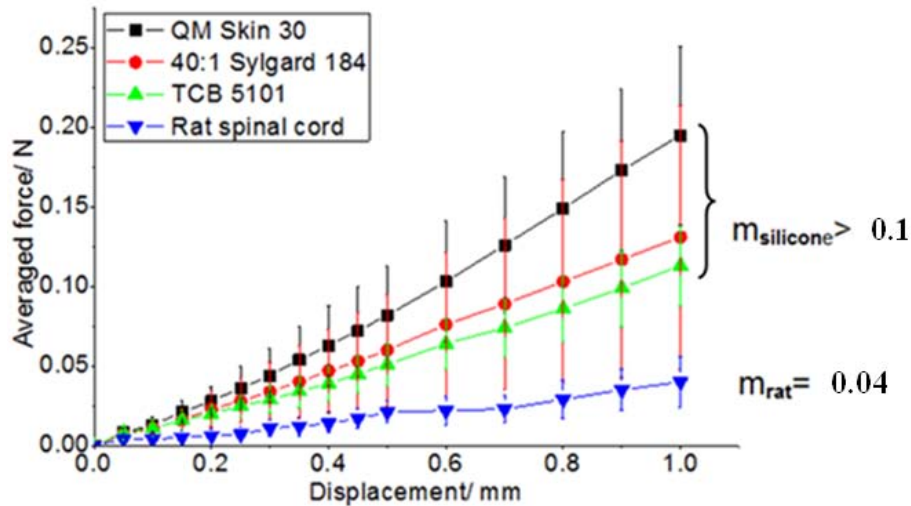


Figure 3-9: The average force of indentation required achieving specific displacements of different silicone cords and the rat spinal cords. The slope of the cords (m) is shown.

The force vs. displacement curve of the 9 wt%, 12 wt%, 15 wt% gelatin in water surrogate cords are shown in Table 3-5, and compared to that of the rat spinal cords in Figure 3-10. ANOVA and Tukey HSD post-hoc analyses were applied to compare the slopes obtained for the rat spinal cords and the cords made from the candidate materials using SPSS (Statistical Package for Social Sciences, IBM, New York, United States). If p-value obtained from the analysis is smaller than 0.05, the differences between the samples are considered statistically significant. The results were summarized in Table 3-6. In each case, the absolute value of the y-intercept was less than 0.01 and the error of the y-intercept was less than 0.002. The average slope obtained for of the curve for the rat spinal cord was $0.04 \text{ N/mm} \pm 0.02$, while for all the three silicones the average slopes were larger than 0.1 N/mm ($0.13 \text{ N/mm} \pm 0.09$, $0.11 \text{ N/mm} \pm 0.03$, and $0.20 \pm 0.06 \text{ N/mm}$ respectively for the 40:1 Sylgard 184, the TCB 5101, and the QM Skin 30), even the smallest of which is still almost three times the target slope.

Therefore, much larger indentation forces were required for each silicone elastomer to achieve the same depth as for the rat spinal cords. The slopes of the indentation curves for each silicone were shown statistically to be significantly different from those obtained for the rat spinal cord. For the gelatin cords, the force required to achieve a specified displacement in each type of gelatin surrogate cord was consistently closer to the force required to achieve the same displacement in the rat spinal cords than for any of the silicone samples. The slopes of the force-displacement curves of the formaldehyde crosslinked 9 wt%, 12 wt%, and 15 wt % gelatin in water cords (0.049 ± 0.004 N/mm, 0.06 ± 0.01 N/mm, and 0.079 ± 0.004 N/mm respectively) were not significantly different from the slopes obtained for the rat spinal cords according to the Tukey post hoc analysis. This was despite the differences in moduli measured by DMA. Moreover, the 12 wt% samples were deemed by an experienced spinal cord physiologist to “feel” more similar to both rat and cat spinal cords than the gelatin cords containing 9 wt% or 15 wt% gelatin in water. Therefore among the 3 different concentrations of gelatin in water samples, the crosslinked 12% gelatin was selected for use in further experiments.

Although hydrated gelatin has been used in the previous literature to engineer a surrogate spinal cord [15], only uncrosslinked gelatin was measured, and the force response to indentation was not considered. This is the first study to evaluate the feasibility of crosslinked gelatin as material to build surrogate spinal cord. It is also

the first attempt to look into the indentation response with respect to the depth of surrogate spinal cords.

Table 3-5: Raw force data for the spinal indentation experiments for formaldehyde crosslinked hydrated gelatin cords and the rat spinal cords. We tested 2 cords of each material. Each cord was tested at 3 different positions except in the case of the rat data with 3 cords tested and one of them only tested at 2 positions and two of them at three positions. The averages and standard deviations at each displacement were calculated.

Displacement (mm)	15% crosslinked gelatin		12% crosslinked gelatin		9% crosslinked gelatin		Rat spinal cord	
	Average force/N	St. Dev /N	Average force/N	St. Dev /N	Average force/N	St. Dev /N	Average force/N	St. Dev /N
0.00	0	0	0	0	0	0	0	0
0.05	0.0033	0.002	0.001	0.001	0.003	0	0.004	0.003
0.10	0.0067	0.002	0.0035	0.002	0.003	0.0006	0.004	0.003
0.15	0.011	0.002	0.0055	0.002	0.005	0.0006	0.005	0.004
0.20	0.015	0.003	0.0085	0.002	0.007	0.0006	0.006	0.004
0.25	0.019	0.003	0.0115	0.004	0.009	0.0006	0.007	0.005
0.30	0.023	0.003	0.0145	0.004	0.012	0.001	0.011	0.005
0.35	0.028	0.003	0.017	0.003	0.014	0.002	0.012	0.006
0.40	0.032	0.004	0.02	0.003	0.016	0.002	0.014	0.006
0.45	0.036	0.005	0.023	0.003	0.019	0.002	0.017	0.006
0.50	0.04	0.004	0.0275	0.005	0.021	0.003	0.021	0.007
0.60	0.048	0.004	0.0335	0.005	0.026	0.002	0.022	0.009
0.70	0.056	0.003	0.0415	0.008	0.031	0.004	0.023	0.009
0.80	0.064	0.003	0.049	0.01	0.034	0.003	0.029	0.012
0.90	0.072	0.003	0.055	0.008	0.039	0.003	0.035	0.013
1.00	0.081	0.003	0.0595	0.0064	0.044	0.002	0.040	0.016

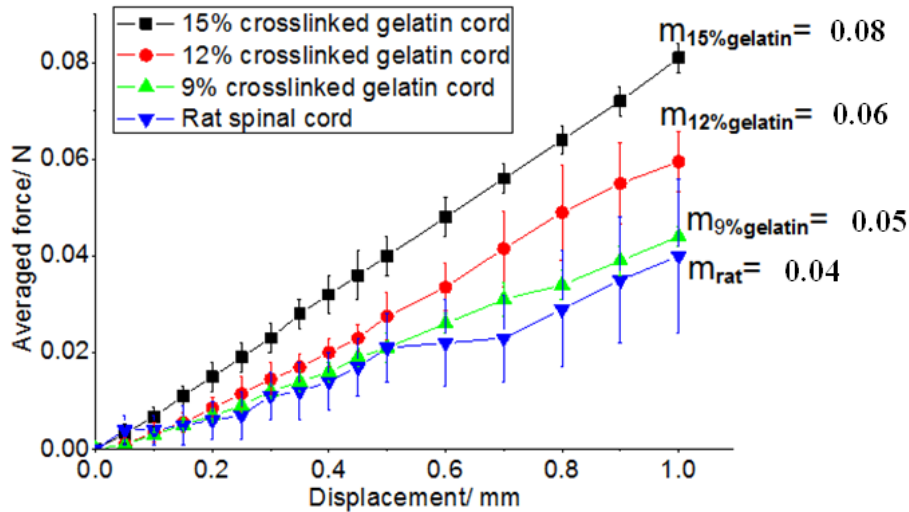


Figure 3-10: The average force of indentation required achieving specific displacements of formaldehyde crosslinked gelatin at different weight percent in water. The curve of the rat spinal cords were plotted for comparisons. The slope of the cords (m) was shown.

Table 3-6: Summary of the statistical analysis. Subgroups are comprised of groups of materials which have slopes which are not statistically different from each other (p -value <0.05), as determined by Tukey post-hoc analysis.

Material	No. of tests	Subgroups with alpha = 0.05		
		1	3	4
Rat spinal cord	8	0.04		
9% gelatin cord	6	0.05		
12% gelatin cord	9	0.06	0.06	
15% gelatin cord	6	0.08	0.08	
TCB 5101	9		0.11	
40:1 Sylgard 184	9		0.13	0.13
QM Skin 30	9			0.20
p-value within subgroup		0.59	0.052	0.09

3.3.4 Frictional Force Testing

To quantify the frictional forces between the spinal cord materials and a standard stainless steel needle, the following tests were performed.

An Instron 4443 Force Tester (Grove City, Pennsylvania, USA) was used to measure the frictional force between a 30 gauge stainless needle and the surface of a variety of surrogate spinal cords (shown in Figure 3-11). For each material, at least two different samples were tested, and each sample was tested at three different locations (one in the middle and one at each end). The frictional force between the needle and two rat spinal cords was also tested. Three spots were tested for each of the two rat spinal cord samples (one in the middle and one at each end).

To obtain these measurements, a 1 cc syringe fitted with a 30 gauge needle was securely mounted to the moving head of the Instron tester. When testing surrogate cords, the tip of the needle was cut to form a blunt edge in order to prevent cutting the cords during testing. Samples were fastened to the stage during testing to prevent moving: silicone cords were taped directly to the stage, whereas gelatin cords were wrapped in plastic wrap to prevent drying, and then fastened with tape. At the start of each test on a surrogate cord, the needle tip was lowered until it was just touching the surface of the cord, and the force was then set to 0 N. The needle was then pushed downward for 5 mm and pulled upward for 4 mm at a pulling rate of 0.3mm/min. The force required to maintain this rate of pulling was measured by the tester. Once completed, the Instron head was moved up and the next spot was positioned under the

needle.

Rat spinal cords were characterized immediately after they were harvested by co-workers in Cell Biology to minimize the degradation that occurs as the samples dry. Characterization of these samples was completed within 45 minutes of removing the cords from the rats. When testing rat spinal cords, a blunt needle was unable to penetrate the sample, and a sharp needle was therefore used. Due to the small dimensions of the rat spinal cords, they were tested in a slightly different loading cycle, in which the needle was pushed into the sample for 2 mm and then pulled out 1 mm at the same pulling speed as for the surrogate cords (0.3 mm/min).

To compare the means of frictional stress of each materials in the needle tests, SPSS 18.0 (Statistical Package for Social Sciences) (IBM, New York, United States) was used for the ANOVA and Turkey post hoc analysis of the peak frictional stresses.

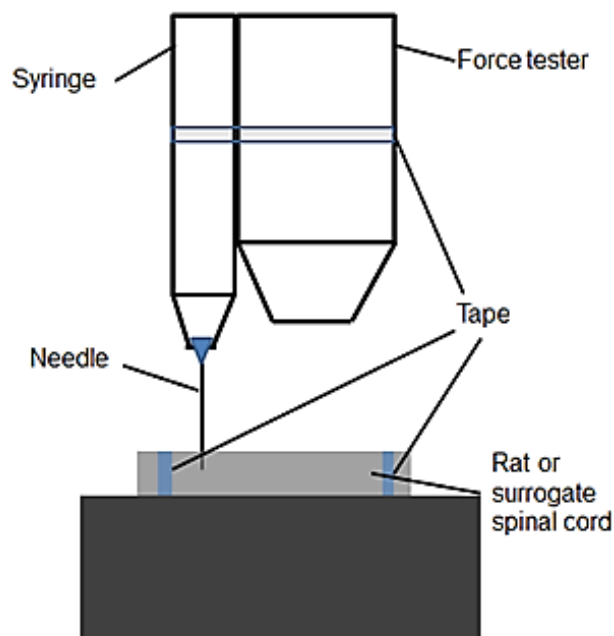


Figure 3-11: Schematic of the frictional force testing set-up during needle insertion.

A representative curve recorded while pulling a needle out of a QM Skin 30 Cord is shown in Figure 3-12. When pulling a needle from a stationary position within the cord, the force increased quickly to a maximum value, and then decreased as the contact area between the cord and the needle decreased. The increase at the beginning of the withdrawal likely occurred as the cord decompressed slightly due to dimpling of the cord during loading. Once this compression was released, a gradual decrease in force was observed as the withdrawal of the needle continued, due to the decrease in contact area between the needle and the cord. Due to differences in rheological properties and in the amount of compression applied at the start of loading, peak forces were achieved at different depths for different samples, and peak forces could therefore not be compared directly between different samples, since these maxima occurred for different contact areas. For each type of cord, the peak frictional stress was therefore calculated based on the peak frictional force observed during the withdrawal of the needle, and the depth at which it occurred. Based on the depth, the area of contact could be calculated using equation (3.2):

$$\delta = \frac{F}{A} = \frac{F_{peak}}{2\pi r_{needle} d_{peak}} \quad (3.2)$$

Where, r_{needle} is the radius of the needle and d_{peak} is the depth of the needle in the cord when peak frictional force occurred.

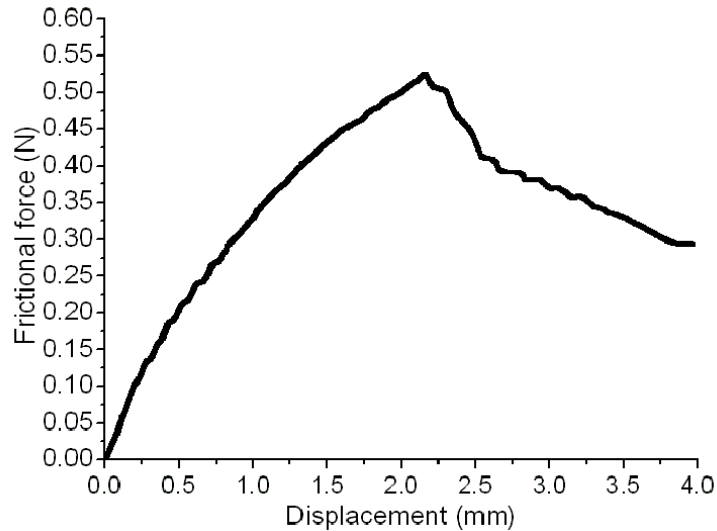


Figure 3-12: A typical force vs. displacement curve for one test recorded from a QM Skin 30 surrogate cord. The maximal force of extraction and the depth at which this force occurs (approximately 0.54 N and 2 mm for the curve shown) are used to calculate the peak frictional stress between the cord and the needle.

The peak frictional stress values for all materials tested are summarized in Table 3-7 and Figure 3-13. The stress at the interface of the needle and the rat spinal cords was very low, and was in fact close to the limit of the sensitivity of the Instron tester used for characterization (0.03N). Of the surrogate materials, the uncrosslinked 12 wt% gelatin samples had the lowest frictional stress, followed by the formaldehyde-crosslinked 12 wt% gelatin samples. ANOVA and Tukey HSD post-hoc analyses showed that the differences between the peak frictional stresses exhibited by the 12 wt % gelatin in water cords (both formaldehyde crosslinked and uncrosslinked) and the rat cords were not significant, while the peak stresses observed for all silicones were significantly different from that observed for the rat cords.

Another problem with the silicone cords is it was impossible to insert the electrode arrays into surrogate cords made by silicones without bending the microwires.

Silicone elastomers were therefore deemed unsuitable for use in the surrogate spinal cord models. The peak stresses for the 12 wt% in water formaldehyde crosslinked gelatin were similar to those of the rat spinal cords, which were also verified by the ANOVA and Tukey post hoc analysis. Therefore, the 12 wt% gelatin in water was deemed to be the most suitable material to mimic the mechanical interactions that take place between microelectrode arrays and the surrogate spinal cord.

Table 3-7: Average peak frictional stresses of the candidate materials.

Material	Average stress (kPa)	Stdev (kPa)
Uncrosslinked gelatin	4.6	1.3
Formaldehyde crosslinked gelatin	32.2	4.3
40/1 PDMS	154.2	27.2
Rat spinal cord	33.9	2.3
QM Skin 30	179.8	32.9
TCB 5101	287.5	8.9

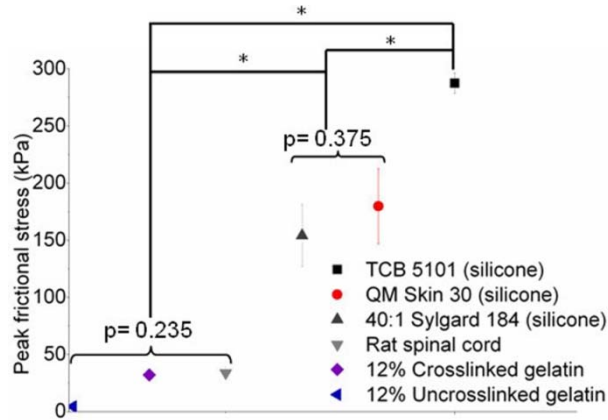


Figure 3-13: Average peak frictional stresses of the candidate surrogate spinal cord materials.

Average \pm standard deviation of peak frictional stresses measured in candidate silicone and gelatin surrogate spinal cords as well as in rat spinal cords. Values are based on 3 locations in at least 3 samples. For each location in the surrogate cords, the needle was inserted to 5 mm and withdrawn for 4 mm. Two rat cords were tested in 3 locations, and for each location the needle was inserted to 2 mm and withdrawn to 1 mm due to the smaller size of the spinal cord. The results of the ANOVA and Turkey post hoc analyses are shown along with the p-values. * indicates groups which have peak frictional forces which are significantly different from each other ($p < 0.05$).

To check whether different loading cycles affects the results, formaldehyde crosslinked 12 wt% gelatin in water and 40:1 Sylgard 184 were measured in both loading cycles and the results were compared in Figure 3-14. It is shown that the results of the formaldehyde crosslinked 12 wt% gelatin in water were very consistent, with small discrepancies. For the results of the 40:1 Sylgard 184, the peak frictional stresses range from approximately 110 kPa to 130 kPa in the longer distance measurements

while those range from approximately 130 kPa to 220 kPa in the shorter distance measurements. This difference is acceptable because in the shorter distance measurements, the values obtained approach the limits of the sensitivity of the instrument. Therefore, the error in these measurements is relatively larger than the longer distance measurements. To further evaluate the differences in the two types of measurements, paired t-tests were taken by and results showed that for both the formaldehyde crosslinked gelatin and 40:1 Sylgard 184, the differences between results obtained from these measurements are not significant. Therefore, the differences in the measurements are acceptable and the peak frictional force obtained from the measurements taken at longer distances can be used for comparison with those obtained in the rat spinal cords at shorter depths.

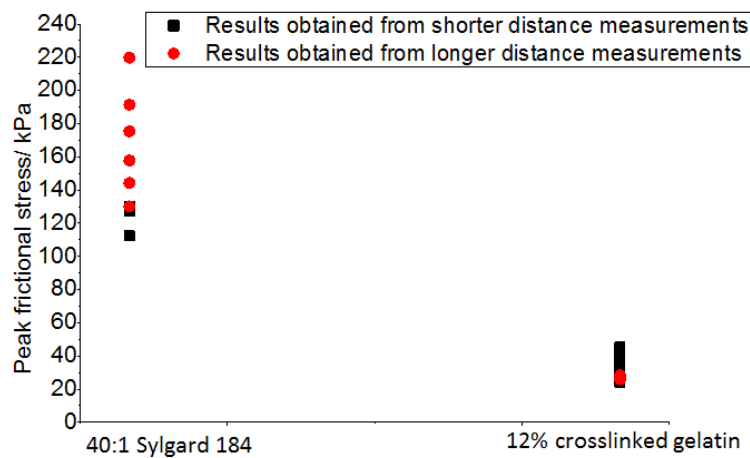


Figure 3-14: Comparisons of the peak frictional stress of formaldehyde crosslinked 12 wt% gelatin in water and 40:1 Sylgard 184 obtained from the shorter distance and longer distance measurements. At least 2 cords were measured for each material in each type of test. The plotted data is raw data obtained from at least 3 measurements at three different spots for each cord.

The surface properties of the surrogate spinal cord must be matched to those of real cords, both to achieve similar frictional stress during implantation and during the relative movements between the electrodes and spinal cords, which would have a large influence on the insertion process and the mechanical interactions that occur between the electrodes and cords, respectively. The surface properties are especially important when using arrays of fine electrodes which have a large surface area to volume ratios, which are preferable for use since electrodes with smaller diameters cause less damage to spinal cord tissue (as discussed in Chapter 1). In the literature, studies have looked at different aspects of insertion behavior, such as the dimpling and compression that occurs during implantation [16] and the force required to penetrate human brain tissue *ex vivo* [17]. However, the frictional stress of between the electrodes and spinal cord tissue has not been studied. This is the first time that the surface properties of surrogate spinal cord and rat spinal cords have been quantified, which adds valuable data to studies of both the surface properties of spinal cords and the insertion behavior of electrode arrays.

One shortcoming of the frictional test is that a 30 gage needle was not representative of the very fine microwires used in the real ISMS implantations. The 30 gage needle was chosen because of the low sensitivity of the Instron machine. In addition, the microwires may be bent when pushing downwards into the sticky silicone surrogate spinal cords. Future tests could be taken on a more sensitive mechanical tester to facilitate the testing of the frictional forces between real electrodes and surrogate spinal

cords. The measurements were taken during the pulling process of the needle instead of inserting, which may also cause a different frictional force behavior.

3.5 Conclusions

Mechanical and surface properties of the candidate materials, silicone elastomers and gelatin hydrogels, were characterized in this chapter to choose the appropriate material for the surrogate spinal cord. The tensile moduli of the candidate materials were measured by the DMA machine and were compared to that of the target modulus which is that of the human spinal cord *ex vivo* [18]. Formaldehyde crosslinked 12 wt% and 15 wt% gelatin in water had the closest moduli according to the results. Although it is shown that the difference between the 12% gelatin and the target modulus is significant in the statistical analysis, the difference is still acceptable due to both differences in test set-ups from the reference paper and the extreme softness of the human spinal cord. Subsequently, indentation tests were taken to quantify the force required to achieve indentation depth of both the candidate materials and the rat spinal cord to have direct comparisons on surrogate cords with the same geometries as real spinal cords. It was found that all the formaldehyde crosslinked gelatin surrogate spinal cords had similar force vs. displacement curves to that of the rat spinal cord according to the ANOVA and Tukey post hoc analysis. In addition, the formaldehyde crosslinked 12 wt% gelatin was found to “feel” the most similar to the real cat and rat spinal cords. Therefore the 12 wt% in water gelatin surrogate spinal cords were chosen for the needle tests.

In the subsequent needle test which quantified the frictional stress of the surrogate and rat spinal cords by pulling a needle out of the cords, the silicone elastomers were found to have significantly higher surface frictional forces than the rat spinal cords. The frictional stresses that occurred at the surface of uncrosslinked and formaldehyde crosslinked 12 wt% gelatin in water were similar to those measured in rat spinal cords, based on the results of the ANOVA and Tukey tests shown in Figure 3-13. However, uncrosslinked gelatin was too fragile to handle to be useful in a surrogate spinal cord. Therefore, the formaldehyde crosslinked 12 wt% gelatin in water was chosen to build a surrogate spinal cord to mimic the mechanical interactions between the electrode arrays for ISMS and the spinal cord.

Chapter 4: Deformation testing of the surrogate spinal cord*

In the previous chapter, formaldehyde crosslinked 12 wt% gelatin in water was chosen as the most suitable material from which to build the surrogate spinal cord, based on the mechanical and surface properties of this material as compared with the real spinal cord. In this chapter, this surrogate cord was used to observe the mechanical interactions that take place between various electrode arrays and the cord that occur during the elongation of the surrogate cord. For patients being treated with ISMS, the implanted electrodes may move relatively to either the spinal cord tissue or the vertebrae of the spine, or even affect the natural deformation of the spinal cord itself. The mechanical properties of the electrode arrays must therefore be carefully chosen and controlled. To observe the stability of microelectrode arrays under ranges of motion to which the spinal cord is typically subjected *in vivo*, surrogate cords were implanted with two different types of electrode arrays and then elongated in a Teflon stand. The behavior of the cord was then observed. For comparison, reference samples without any electrodes implanted were also analyzed.

4.1 Deformation of human spinal cord

During daily life, the spinal cord undergoes a range of deformation, including torsion, flexion, and elongation. To mimic the mechanical interactions between the electrodes and the cord, the surrogate cord must be deformed within the same range experienced

* *Parts of this chapter have been submitted for publication in the Annals of Biomedical Engineering (November 11, 2011)*

by a spinal cord during natural daily motion. Yuan *et al.* [1] quantified the deformation of cervical spinal cord with the participation of adult volunteers during different increments of flexion up to 55° by MRI. Both the amounts of strain experienced on the posterior and anterior sides were measured for each increment by MRI. The results showed that the maximum strain varied between 6.8% and 13.6% on the posterior surface, while those in the anterior surface were smaller, ranging from 3.7% to 8.7% (shown in Figure 4-1). Another study was taken to measure the amount of deformation during natural extension and flexion *in vivo* by Margulies *et al.* [2]. In their work, the deformation of the spine of volunteers was imaged by MRI during the flexion and extension at slow neck strain rates. The stretch ratio was analyzed from the images. It was found that the largest average stretch ratio was 1.12 at segment of C7. In my work, the tensile deformation strain was therefore chosen to be 12%.

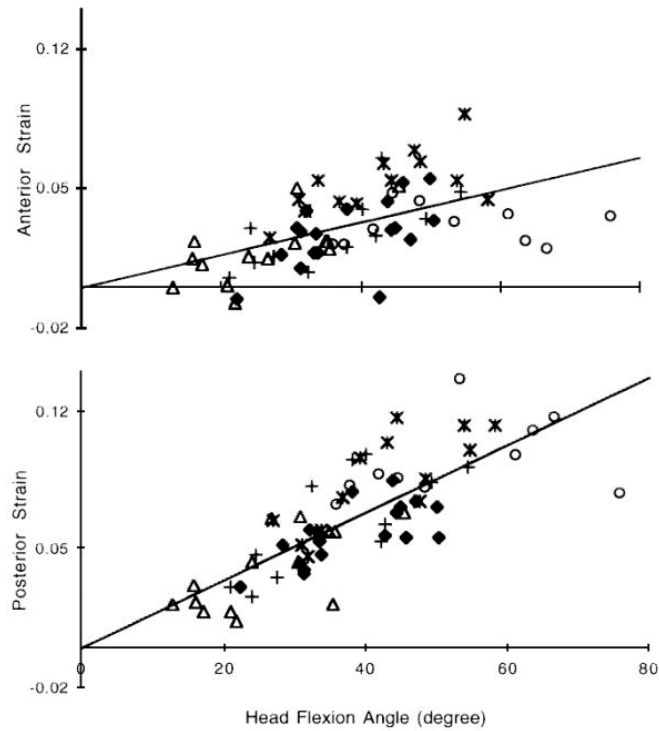


Figure 4-1: Strains of anterior and posterior surfaces of the entire cervical spinal cord at different head flexion angle of the five volunteers. Each symbol represents one volunteer. Slopes of lines are average slopes for all the subjects [1]. Reprinted with permission from Wolters Kluwer Health.

4.2 Electrodes for the deformation tests

4.2.1 Electrode arrays with individual wires

The first type of electrode array investigated consists of independent microwires. The array is comprised of 8 individual 30 μm stainless steel microwires. For ISMS, these wires are typically implanted in two lengthwise rows on the surface of the surrogate spinal cords, at 2 mm to 3 mm interval (shown in Figure 4-2). The advantage of using individual microwires is that they are relatively inexpensive and easy to fabricate.

However, the implantation process can be tedious and difficult, requiring careful work by the surgeon. The implantation process can therefore be very long, which can cause the surgeon to become fatigued, and which also increases the stress on the patient.

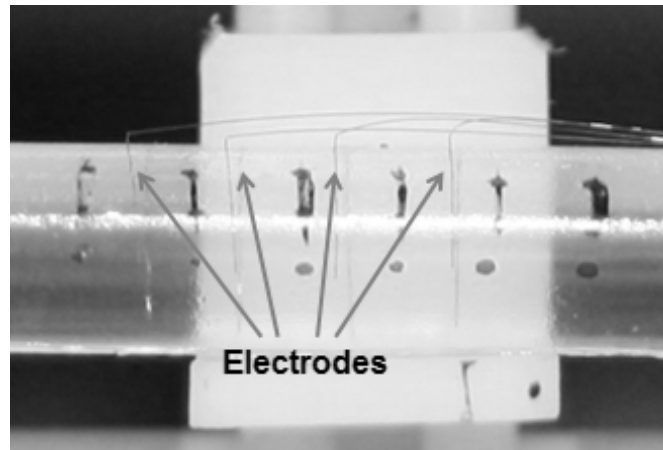


Figure 4-2: Picture of the individual microwires implanted in the formaldehyde crosslinked 12 wt% gelatin in water surrogate cord.

4.2.2 The McCreery array (solid base array)

The second microelectrode array to be tested is a customized McCreery array. It consists of a stiff epoxy base, which holds eight microelectrodes in two rows at 3 mm intervals along the length of the cord (shown in Figure 4-3). The microelectrodes employed in the McCreery array are 75 μm in diameter. This array is of interest because of the simplicity with which it can be implanted, as 8 electrodes are implanted in only one insertion. Another advantage is that this array can improve targeting during insertion since the relative positions of the electrodes are fixed by the base, and these positions can be custom designed based on MRI images of the cord. The McCreery array is commonly used in brain implants as was discussed in section 1.4.3.

In addition, it has been used for short-term implantation in feline spines [3]. Although the solid base can prevent the electrodes from buckling or dislodging during the insertion, their mechanical compatibility with the soft spinal cord is unproven. The McCreery array has been used previously by our co-workers in the Department of Cell Biology (University of Alberta) to restore standing and walking functions in cats. Arrays were implanted in two cats, each of whom exhibited improved function through the use of ISMS. However, after two weeks, the cats were no longer able to stand and walk. Histology tests were conducted to investigate the cause, and it was found that the tissue in the spinal cord was damaged, likely due to the solid base of the arrays. Further work is required to understand why this damage occurred, and some of the results described later in this chapter will help to provide insight into this damage.

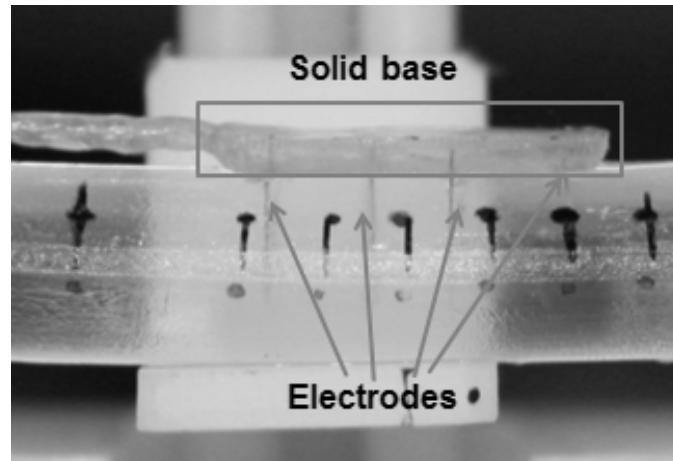


Figure 4-3: Picture of the McCreery arrays implanted in the formaldehyde crosslinked 12 wt% gelatin surrogate spinal cord. The McCreery array contains two rows, although only one can be observed sideways in this picture.

4.3 Methods and results

This section begins by describing the methods used to test the deformation of the surrogate cord itself when implanted with the two types of electrode arrays described above. The results are then presented.

To observe the deformation of the surrogate cord, camera images were used to record the strains between different parts of the surrogate cord as it was elongated by 12% in a Teflon stand, as shown in Figure 4-4. Ideally, the surrogate cord would deform uniformly with a strain of 12% along the length.

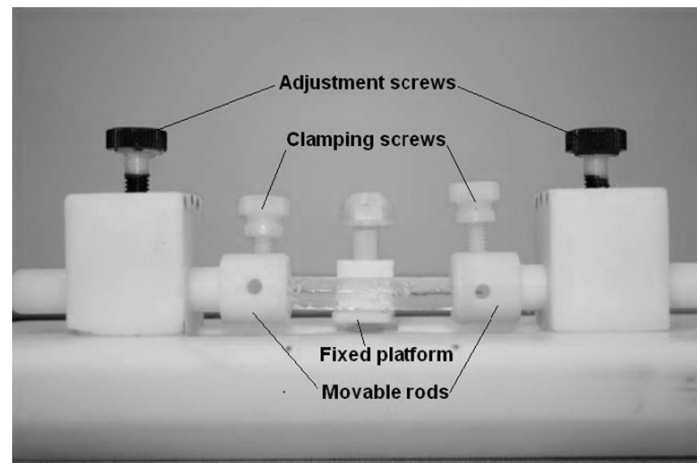


Figure 4-4: Picture of the Teflon stand for the deformation testing. The stand is comprised of a fixed central platform, which can be raised or lowered to support the middle section of the surrogate cord, and two adjustable rods, which can be moved laterally to apply tension to the cord.

To facilitate the clamping of the cord within the stand, the ends of the cords were coated with a thick layer of epoxy (MG Chemicals Fast Set Epoxy 8332, Surrey, British Columbia, Canada), which was allowed to set overnight at 4°C. The cords were then

soaked in water at 4°C for 24 hours before experimentation to ensure that they were thoroughly hydrated and to minimize the drying before the measurements. The extra water absorbed overnight provided a buffer against the drying that would occur during the set-up and completion of the experiment the next day. To validate this approach, the modulus, indentation behavior, and frictional properties of cords soaked overnight in water were also tested on three different samples. The results of the moduli, indentation tests and needle tests of gelatin after soaking in water were compared to those of the fresh gelatin. Paired t-tests were used to evaluate the statistical differences between the results of each test for fresh gelatin and for gelatin soaked in water. If the p-value obtained was smaller than 0.05, the differences were considered statistically significant. Only minor changes were seen: the modulus decreased from 65 ± 6 kPa to 58 ± 3 kPa (paired t-test, $p = 0.052$), the peak frictional stress increased from 23 ± 3 kPa to 29 ± 4 kPa (paired t-test, $p = 0.08$), and the force of indentation required to achieve a 0.5 mm displacement increased slightly from 0.028 ± 0.002 N to 0.031 ± 0.003 N (paired t-test, $p = 0.2$). Due to gradual drying of the samples, it is expected that the final properties of the surrogate cords were somewhere between those of the crosslinked 12 wt% gelatin characterized above, and the crosslinked 12 wt% gelatin samples which had been soaked in water. Therefore, the properties between the fresh gelatin and after the gelatin soaked in water were considered to be similar. After soaking, surrogate cords were implanted with the appropriate electrodes, a procedure that took up to 45 minutes for the case of individual electrodes. To visualize

the distribution of strain within the cord under elongation, four pairs of reference dots were drawn on the surface of the cord in India ink (as shown in Figure 4-5). The cord was loaded in the Teflon stand and was elongated by 12% of its initial length. This strain was reported to be the maximal strain of a human spinal cord during flexion, as determined by MRI [2]. At least three pictures of each configuration were taken using a Canon EOS 1000D camera (Rockville, Maryland, USA) as the cords were relaxed and stretched. The distance between the reference markings was measured before and after the deformation was applied from the pictures using both Adobe Illustrator and AxioVision software, and the results were used to determine the resulting strain in different parts of the cord. To calculate the distance between markings in absolute units (mm), the dimensions of the stand itself were used to calibrate the measurements. Surrogate spinal cords implanted with individual microwires and McCreery array were tested. Each set of measurements was repeated with at least two surrogate cords for each array type. To compare the deformation of the surrogate cord itself, the same tests were also performed on two reference surrogate cords without any electrodes implanted.

The strains between different parts of the cord were obtained by calculating the distance changes between the reference dots (L1, L2, L3, L4, and L5, as shown in Figure 4-5d).

To compare the deformation behavior of surrogate spinal cords implanted with different types of arrays, ANOVA and Tukey post hoc test were taken using SPSS (Statistics Package for Social Sciences, IBM, New York, United States) on surrogate

cords implanted with different electrodes and the reference cords on the strain raw data of L1, L2, L3, L4 and L5. P-values of less than 0.05 were deemed to be significantly different.

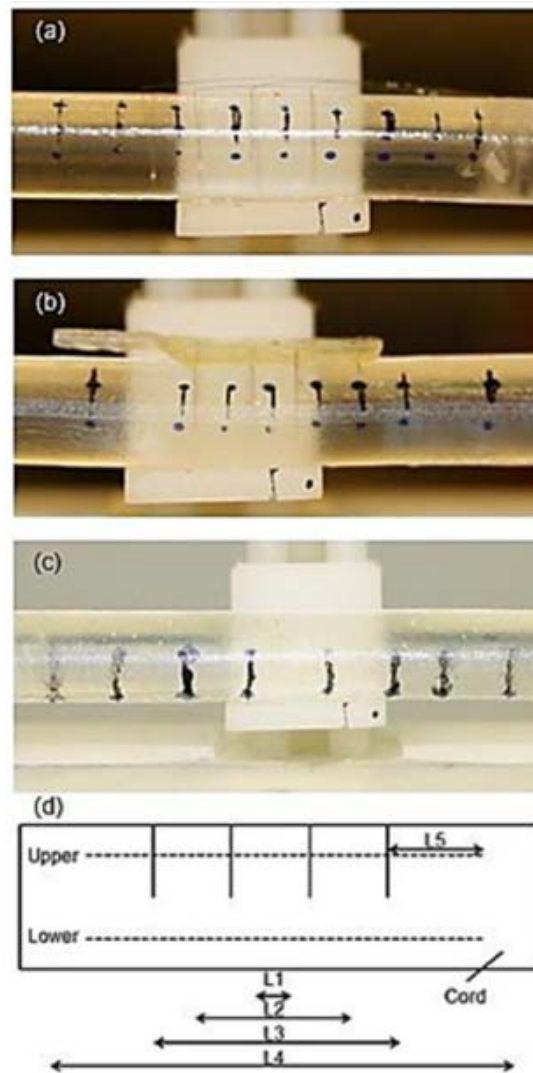


Figure 4-5: Surrogate spinal cords (a) implanted with individual microwires; (b) implanted with electrodes held with solid base; and (c) reference cord with no implants. The schematic diagram (d) indicates the labeling of the ink reference markers used to measure the deformation in the cord when strain was applied.

The results of the reference cords without any array implanted are summarized in Table 4-1 and Figure 4-6. The deformation in these reference surrogate cords (which were not implanted with electrodes) was uniform throughout the cord, ranging from $10 \pm 1\%$ to $13 \pm 1\%$. The 1% uncertainty in all measurements was due to the distortion caused by the lens of the camera, and due to the difficulty of both achieving perfect focus for all relevant planes on the curved surface of the cord and measuring lengths from a digital photograph. Furthermore, the applied deformation may have been non-uniformly distributed through the sample due to the method with which the sample was clamped, causing larger deformations to occur near the ends and smaller deformations towards the center of the sample. Collectively, this accounts for why identical amounts of strain were not seen between each set of reference markers on the reference cord.

Table 4-1: Observed strain in reference samples (without electrodes) under 12% tension.

#	L1 Upper /%	L1 Lower /%	L2 Upper /%	L2 Lower /%	L3 Upper /%	L3 Lower /%	L4 Upper /%	L4 Lower /%	L5 Upper /%	L5 Lower /%
1	11±1	11±1	12±1	11±1	12±1	13±1	12±1	12±1	13±1	13±1
2	10±1	10±1	11±1	10±1	11±1	10±1	11±1	10±1	12±1	13±1

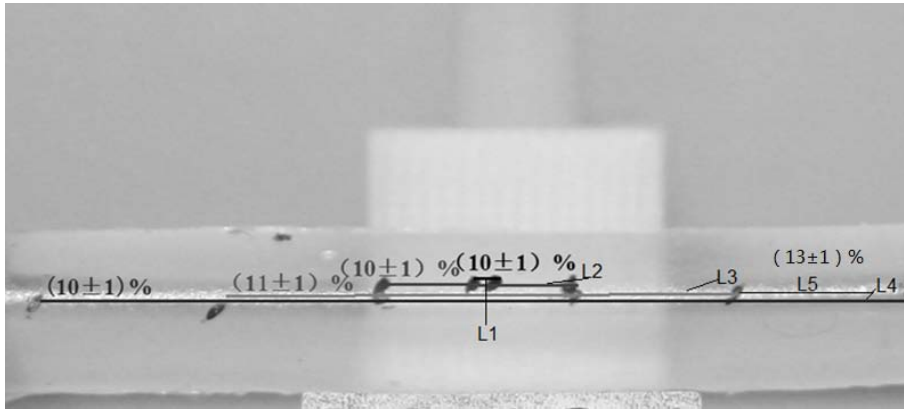


Figure 4-6: Strain of L1, L2, L3, L4 and L5 of surrogate cord without electrodes implanted under 12% tension. Two cords were tested and at least 3 pictures were taken both before and after the deformation. The strains of the upper and lower parts of each part were similar. The values of strains were averaged and shown in this figure. The 1% error is also shown.

The calculated strains of the surrogate cords with individual microwires are shown in Table 4-2. The averaged strain profile of the surrogate spinal cord implanted with individual microwires is shown in Figure 4-7. The strains between different pairs of dots for the cord were almost uniform between the different reference dots, and along the upper and lower parts of the cord. All strains observed were similar to the applied strain, and to those seen for the reference cords (given the error is 1%). ANOVA and Tukey post-hoc analyses were used to compare the strains observed between the same sets of reference markers for the cords implanted with individual wires and the reference cords (without wires). The following p-values were obtained by comparing the average values measured for each set of cords: L1 (p=0.3), L2 (p=0.4), L3 (p=0.06), L4 (p=0.4), L5 (p=0.08), indicating that no statistically significant differences were observed. This shows that cords implanted with individual microwires and cords

without arrays underwent similar mechanical responses to the applied deformation without any array implanted. Therefore, there is little mechanical influence of the individual microwires in terms of the deformation of the surrogate spinal cord. The cord can deform freely without impedance from the electrodes.

Table 4-2: Observed strain in reference samples with individual microwires under 12% tension.

#	L1 Upper /%	L1 Lower /%	L2 Upper /%	L2 Lower /%	L3 Upper /%	L3 Lower /%	L4 Upper /%	L4 Lower /%	L5 Upper /%	L5 Lower /%
1	13±1	11±1	9±1	9±1	10±1	11±1	11±1	11±1	12±1	10±1
2	10±1	13±1	10±1	11±1	10±1	9±1	10±1	9±1	12±1	11±1

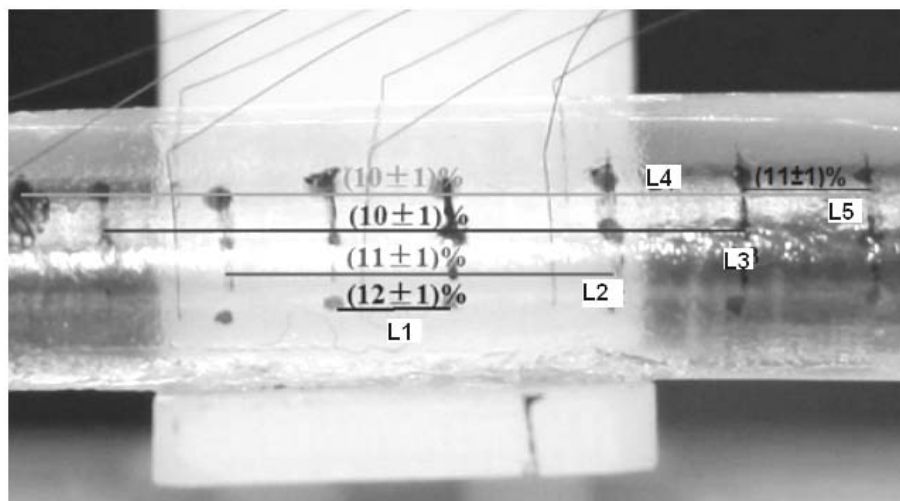


Figure 4-7: Strain of L1, L2, L3, L4 and L5 of surrogate spinal cord with individual microwires implanted under 12% tension. Two cords were tested and at least 3 pictures were taken both before and after the deformation. The strain of the upper and lower parts of each part was similar. The values of strains were averaged and plotted. The 1% error was plotted as well.

No significant difference was seen between upper and lower reference dots.

The calculated strains of the surrogate spinal cord with solid base (McCreery array) are shown in Table 4-3. The averaged strain profile of the cord and the strain of the upper and lower part of each part of surrogate spinal cords with McCreery arrays are shown in Figure 4-8 (a) and (b), respectively. To provide a general comparison of the strains of the three different surrogate cords, the strains between L1 to L5 were plotted in Figure 4-9. While the strains of both the reference cords and cords implanted with individual microwires were uniform, for the cords implanted with McCreery array, the strain increased from the inner part to the outer part of the cord. The strain under the middle part (L1) of the solid base is only $4\pm 1\%$, which is much lower than the applied strain. The strain between the dots on the edge of the solid base (L3) is $8\pm 1\%$, and the strain between the two edges (L4) was $9\pm 1\%$. To achieve a total strain of 12% overall, a much larger deformation occurred in the region outside the array (L5), whose strain was $14\pm 1\%$ to $16\pm 1\%$.

ANOVA and Tukey post-hoc analyses returned the following p-values for the reference cord and the cord embedded with the McCreery array: Upper: L1 ($p < 0.0001$), L2 ($p < 0.001$), L3 ($p < 0.0001$), L4 ($p=0.2$), L5 ($p < 0.001$), Lower: L1 ($p < 0.001$), L2 ($p < 0.001$), L3 ($p < 0.001$), L4 ($p=0.3$), L5 ($p < 0.001$). The only set of markers which underwent a deformation that was not significantly different from the reference cord was L4. These were the longest set of markers, and took into account both the area under the array (which underwent smaller strain) and the area flanking the array (which underwent larger strain) to accommodate the overall strain of 12%. The strain of the

upper part in the same region was consistently smaller than that of the lower part under the solid base. This occurred because the solid base, which touched the top surface of the cord, constrained the top surface of the cord. Further from the base (along the lower reference line) this effect was less pronounced. Overall, the solid base prevented the cord from deforming uniformly along both the depth and length of the cord.

Table 4-3: Observed strain in reference samples with solid base array under 12% tension.

#	L1 Upper/ %	L1 Lower /%	L2 Upper/ %	L2 Lower /%	L3 Upper/ %	L3 Lower /%	L4 Upper/ %	L4 Lower /%	L5 Upper/ %	L5 Lower /%
1	3±1	4±1	6±1	9±1	6±1	6±1	10±1	10±1	15±1	14±1
2	3±1	5±1	5±1	7±1	7±1	7±1	8±1	8±1	16±1	14±1

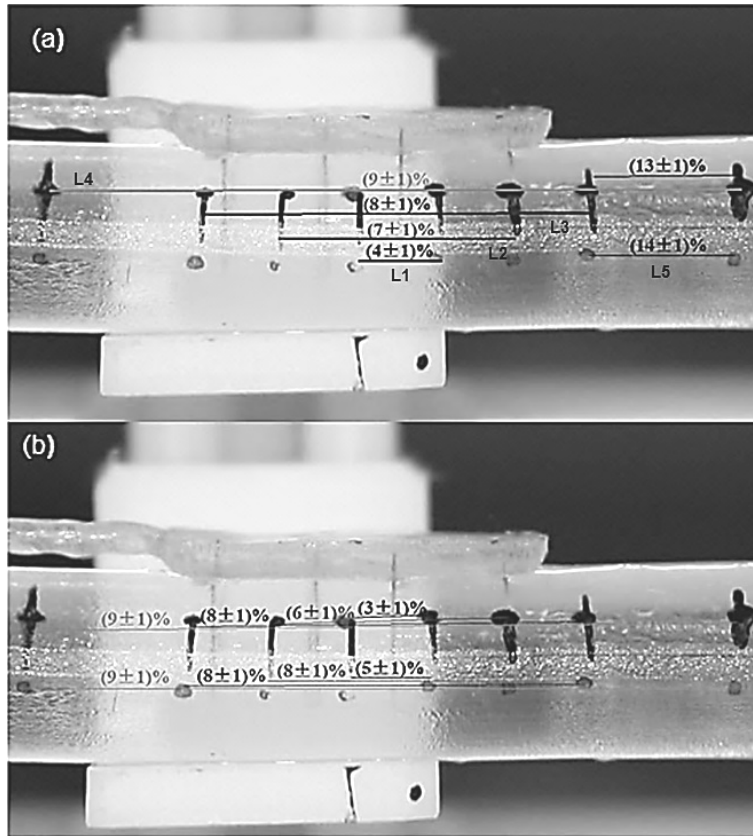


Figure 4-8: Strains observed in surrogate spinal cords implanted with McCreery arrays, subjected to 12 % tension. (a) Strains observed between reference markers L1, L2, L3, L4 and L5 (averaged between the upper and lower rows). (b) Strains observed between reference markers L1, L2, L3, L4 and L5 along upper and lower portions of the cord. The 1% error is shown as well.

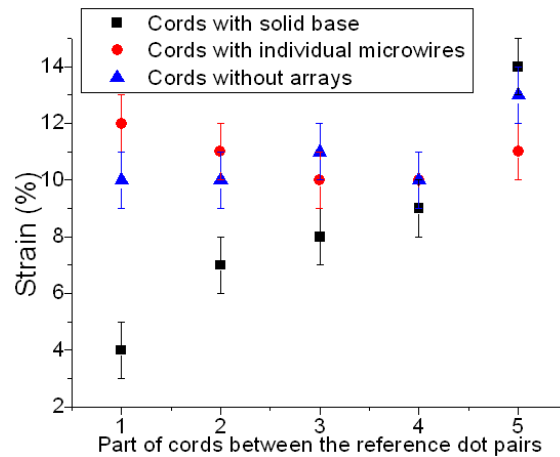


Figure 4-9: Comparisons of the strains of the cord with individual microwires, solid base array and without any array between L1 to L5.

To verify the strain profiles calculated from the images, the strain observed between the L4 markers (corresponding to the entire length of the cord) was compared with the sum of strains seen in L3 and L5 (weighted by the overall length of these regions). The weighted strains (ϵ_4) were calculated by Equation 4-1 and compared to the values obtained directly from the image analyses (L4), which is shown in Table 4-4, along with similar calculations for the reference cord and the cord implanted with individual wires.

Taking into the 1% error into account, the calculated strains were very consistent with the observed strains in the image. This verified the image analyses in the deformation tests, and showed that for the McCreery arrays the decreased deformation under the solid base was compensated for by increased deformation outside of the base.

$$\begin{aligned}\varepsilon_{L4} &= \frac{(\varepsilon_{L3} \times L3 + \varepsilon_{L5} \times L5)}{L3 + L5} \times 100\% \\ &= \left(\frac{\overline{\varepsilon_{L3}} L3 + \overline{\varepsilon_{L5}} L5}{L3 + L5} \right) \times 100\% \pm 1\%\end{aligned}\tag{4.1}$$

Table 4-4: Comparisons of the calculated strains to the observed strains of the surrogate spinal cord with the individual microwires, solid base array and without any arrays (reference cord).

	Reference Cord 1	Reference Cord 2	Individual Microwires Cord 1	Individual Microwires Cord 2	Solid Base Cord 1	Solid base Cord 2
Calculated Strain (%)	12±1	11±1	10±1	9±1	10±1	9±1
Observed strain (%)	12±1	11±1	11±1	9±1	10±1	8±1

4.4 Discussion and conclusions

4.4.1 Discussion

Bamford *et al.* [4] have previously studied the biological changes that occur in the spinal cord tissue when individual microwires are implanted in the spine and used for ISMS. In this study, rats were transected, implanted with individual microwires and the rat spinal cords were stimulated for 4 hours a day for 30 days. The results showed only minimal tissue damage resulted during stimulation. These results complement the findings from the present work, which suggest that individual microwire arrays move with the cord and should not cause damage due to mechanical interactions.

The second types of array, McCreery array is representative of the types of stiff electrode arrays commonly used in deep brain stimulation [5]. Although it has been

used for short-term implantation in feline spines [3], the finding in that study showed that this type of array cause little histological change to the spinal cord tissue over time. Our co-workers have used this type of array in feline spinal cord and observed tissue damage after two weeks' implantation. My results help to explain why. While fairly uniform deformations occurred between all sets of reference markers for the reference cords (without implants) and the cords implanted with individual wires, for the cords implanted with arrays with solid bases, significantly lower deformations occurred beneath the middle of the solid base ($3 \pm 1\%$ to $7 \pm 1\%$) compared to the applied strain (12%). The strains increased from the inner part to the outer part of the cord beneath the base, with the strains of $9 \pm 1\%$ observed along L4, which includes both the area beneath the base and surrounding the base. The above results suggest that the McCreery array impeded the uniform deformation of the cord from stretching, because the stiff, glassy base interacted with the surrogate cord mechanically and prevented it from deforming freely. Therefore, during deformation, the ends of the electrodes which were connected to the solid base were fixed in place, while the tips of the electrodes (deep inside the surrogate spinal cord) move with the spinal cord. It is expected that shear stress would occur at the interface between the electrodes and the cords because of the relative movements between them. During long-term implantations, this stress could potentially result in damage of the spinal cord tissue (by causing tearing or other mechanical damage to cells in the region). The McCreery array, in this respect, is not appropriate for the long-term implantation for ISMS.

When ISMS electrodes are implanted for long-term use, they will be subjected to thousands of cycles of strain and relaxation. During these cycles, the cord may become damaged due to interactions that take place between the hard electrodes and the soft cord. This damage may include tearing, or other types of mechanical damage to the cells. Therefore the McCreery array is not ideal for use in ISMS technique in terms of mechanical stability.

Apart from testing the existing electrode arrays, the surrogate cord was also used to test an array with a flexible base developed by our collaborator Imad Khaled (Mechanical Engineering Department, University of Alberta) (shown in Figure 4-10). In tests on his array, it was found that much larger deformations could be achieved in the region beneath the base than with the McCreery arrays. This showed that the surrogate cord is not only useful in testing of existing arrays, but also for testing the design of new electrode arrays being developed for ISMS.

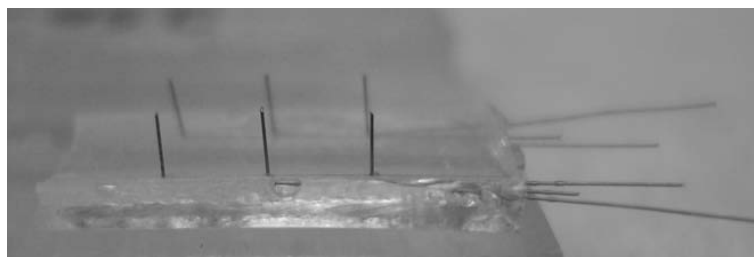


Figure 4-10: Picture of the flexible array developed by Imad Khaled.

In future studies, it would also be advantageous to be able to image both the relative motion between the electrodes and the surrogate cord. The movement of the electrodes themselves could not easily be resolved in the images used to evaluate the

deformation of the surrogate cords. The orientation of the electrodes themselves could perhaps be achieved using a technique such as micro-CT, which should be able to image metal electrodes inside of the cord without distortion. In addition, it would be useful to conduct experiments in an animal model.

4.4.2 Conclusion

In this chapter, a method to evaluate the mechanical stability of ISMS electrode arrays within a surrogate spinal cord was presented for the first time, enabling the preliminary testing of electrode arrays *in vitro* without harvesting real animal spinal cords. This technique is valuable in terms of testing the long-time mechanical safety issue of the electrode arrays which can be used in ISMS.

Chapter 5 Conclusion

The purpose of the research described in this thesis was to develop a proof-of-concept surrogate spinal cord to test the mechanical stability of implantable microelectrode arrays for use in intraspinal microstimulation (ISMS). In the first phase of the work, the mechanical and surface properties of a variety of materials were characterized to identify the material which best mimicked an actual spinal cord. Three silicone elastomers (in different elastomer:crosslinker ratios) and uncrosslinked and formaldehyde crosslinked hydrated gelatin at three different concentrations were evaluated using a variety of techniques, for comparison with the real spinal cord. The tensile moduli of the candidate materials were measured by DMA and compared to the modulus of the human spinal cord *in vitro* (reported in the literature). To compare the mechanical behavior of candidate material samples directly to real spinal cords, candidate materials were molded into spinal-cord like shapes, and the force required to indent each sample up to 1 mm was measured and compared with the force required to indent an *in vitro* rat spinal cord. The surface properties of candidate materials and actual rat spinal cords were then quantified by pulling a needle out of each sample at a controlled rate. While silicone have been used previously to produce the surrogate spinal cord in the literature [1-3], the high surface friction measured during the needle test makes these materials unsuitable for testing the mechanical stability of intraspinal implants. Formaldehyde crosslinked 12 wt% gelatin in water was chosen to construct the surrogate spinal cords, despite the fact that this material dries

gradually during the handling process, and therefore must be worked with carefully.

After building the proper surrogate spinal cord, the mechanical stability of electrode arrays implanted into the cord were tested. Two types of arrays were tested: the first array consisted of individual wires, and the second array had a solid base connecting the wires (McCreery array). The deformation of the surrogate cords was measured by imaging the cord with reference dots on the surface before and during tensile deformation. It was found that the individual microwires had little influence to the deformation of the cord itself, while the elongation of the surrogate cords was impeded by the solid base of the McCreery array. We also showed that the surrogate cord can be used to test new electrode array designs developed by our collaborators.

5.1 Future Work

There are many future directions this research could take. In my work, the indentation test and needle test were performed on *ex vivo* rat spinal cords for comparison with the candidate materials. In the next phase of the work, these experiments should be repeated with cat spinal cords (rather than rat spinal cords), since the preliminary ISMS experiments are typically carried out on cats. This would allow for better comparison with the results of these animal experiments. In addition, the spinal cord was treated as a homogeneous material, while in reality, the spinal cord is complex with different regions with different properties. the whole spinal cord includes both *gray* and *white matter*, and from the literature it is known that *gray matter* is actually more rigid but fragile than the *white matter*

through the differences in terms of modulus is not large [4]. Within each individual region, further anisotropies may also exist due to the organization of the cells themselves. Therefore, in future work it is desirable to take these differences into account to mimic the mechanical properties of the spinal cord more accurately. While the surrogate cord presented in this thesis mimics the human spinal cord in vitro without *pia matter*, The simulation would be more accurate if the “pia ” could be added in the surrogate spinal cord. To achieve this, future study could be coating the surrogate spinal cord. In the long term, it is desirable to evaluate both mechanical and biological interactions between the spinal cord and implants to get a more comprehensive understanding of the safety issue of the electrode arrays. Therefore another direction for future work is the addition of cells to the model. Culturing relevant cells in a three-dimensional configuration would allow their response to various implants to be studied during relevant mechanical deformations.

In terms of the deformation test set-up, one drawback of this study is that it is not possible to compare the deformation behavior of surrogate spinal cords implanted with arrays directly with real, *ex vivo* spinal cords implanted with electrode arrays. This is due to both to limited availability of real cords, and to the fact that the properties of actual spinal cords change significantly after both death and removal, as described in Chapter 1. Further research would be useful to measure the deformation of real spinal cord with implanted arrays.

Currently in the deformation tests, only the strain profile of the surrogate spinal cord was evaluated. To examine the mechanical interactions between the electrode arrays and surrogate spinal cord, the movement of each electrode is also an important factor. Therefore, future research could be testing the mechanical movements of the electrode arrays using micro-CT technique and compare with the strain profile of the surrogate spinal cord. In this way, the relative movements could be evaluated. In addition, in the testing described in this thesis, only tensile deformation is considered. Further research might be desired to test the deformation behaviors of surrogate spinal cord under other typical deformation modes such as bending and twisting.

5.2 Concluding Remarks

The proof-of-concept surrogate spinal cord presented in this thesis provides a valuable to test the preliminary stage designed microelectrode arrays *in vitro*. This system could both save money and minimize the use of animals for testing. While different surrogate spinal cord models have been described previously in the literature, this study is the first attempt to build surrogate cord looking into the surface properties of the cord for the considerations of the insertion behavior and mechanical interactions between the cord and the electrode arrays.

In the future, the surrogate cords which I have developed will be used to screen new designs for electrode arrays for use in ISMS currently being developed by my group and collaborators. After validating these models in the surrogate cord, they may be evaluated in *ex vivo* and *in vitro* models. In addition, in the future our